DISSERTATION

I. GROUND-STATE ASSOCIATION BETWEEN PHENOTHIAZINE AND TRIS(DIIMINE)RUTHENIUM(II) COMPLEXES: ITS ROLE IN HIGHLY EFFICIENT PHOTOINDUCED CHARGE SEPARATION. II. LIGAND MODIFICATIONS OF COBALT COMPLEXES TO INCREASE EFFICIENCY OF ELECTRON-TRANSFER MEDIATORS IN DYE-SENSITIZED SOLAR CELLS

Submitted by

John Weber

Department of Chemistry

In partial fulfillment of the requirements

For the Degree of Doctor of Philosophy

Colorado State University

Fort Collins, Colorado

Spring 2012

Doctoral Committee:

Advisor: C. Michael Elliott

Anthony Rappe
Nancy Levinger
Robert Woody
Alan Van Orden

ABSTRACT

I. GROUND-STATE ASSOCIATION BETWEEN PHENOTHIAZINE AND TRIS(DIIMINE)RUTHENIUM(II) COMPLEXES: ITS ROLE IN HIGHLY EFFICIENT PHOTOINDUCED CHARGE SEPERATION. II. LIGAND MODIFICATIONS OF COBALT COMPLEXES TO INCREASE EFFICIENCY OF ELECTRON-TRANSFER MEDIATORS IN DYE SENSITIZED SOLAR CELLS

Supramolecular triad assemblies consisting of a central trisbipyridineruthenium(II) chromophore (C^{2+}), with one or more appended phenothiazine electron donors (D) and a diquat-type electron acceptor (A^{2+}) have been shown to form long-lived photoinduced charge separated states (CSS) with unusually high quantum efficiency. Up to now, there has been no explanation for why such large efficiencies (often close to unity) are achieved from these systems when other, seemingly similar, systems are often much less efficient. In the present study, using a bimolecular system consisting of chromophore-acceptor diad (C^{2+}-A^{2+}) and an N-methylphenothiazine donor we demonstrate that a ground-state association exists between the RuL_3^{2+} and the phenothiazine prior to photoexcitation. It is this association process that is responsible for the efficient CSS formation in the bimolecular system and, by inference, also must be an essential factor in the fully intramolecular process occurring with the D-C^{2+}-A^{2+} triad analogs.

Alkyl-substituted bipyridine ligands in cobalt II/III complexes were modified in order to serve as efficient electron-transfer mediators in dye-sensitized solar cells. Attempts at halogen

substitution reactions are described. Ultimately isopropyl groups appended to bipyridine ligands were modified by introducing a hydroxyl group at the benzylic position. The electrochemical behavior of the modified ligand is described, as well as its performance as part of a cobalt complex electron-transfer mediator in dye-sensitized solar cells.

TABLE OF CONTENTS

LIST OF ILLUSTRATIONS

LIST OF ABBREVIATIONS AND SYMBOLS

A	electron acceptor
ACN	acetonitrile
BPO	benzoyl peroxide (radical initiator)
bpy	2,2’ –bipyridine
C	chromophore
CSS	charge separated state
CT	charge transfer state or charge transfer interaction
DCM	dichloromethane
dmb	4,4’ –dimethyl – 2, 2’-bipyridine
D	electron donor
D	deuterium (in a chemical formula)
D-C-A	donor-chromophore-acceptor systems
ΔAbs.	differential absorbance or transient absorption of CS
DSSC	dye-sensitized solar cell
DQ	diquaternary amine
$\mathbf{E^o}$	standard reduction potential
$\mathbf{E_{1/2}}$	half-wave potential of the anodic and cathodic peak potentials
ES	excited state
$\mathbf{ES^+}$	electrospray ionization mass spectroscopy
GS	ground state
$\boldsymbol{\lambda_{max}}$	maximum absorption or emission wavelength
L	ligand

LDA	lithium diisopropylamide
N-MePTZ	methyl phenothiazine
^{n}MLCT	metal to ligand charge transfer; n refers to the spin multiplicity of the state
N3	cis-diisothiocyanatobis(2, 2' – bipyridine-4,4'-dicarboxylic acid) ruthenium(II)
NBS	n-bromosuccinimide
NCS	n-chlorosuccinimide
NFSI	n-Fluorobenzenesulfonimide
Φ_{CSS}	efficiency of charge separated state formation
phen	1,10-phenanthroline
δ	ppm (x axis position from NMR)
PMT	photomultiplier tube
PTZ	phenothiazine (an electron donor)
PQ	paraquat (quaternary amines in the *para* ring position)
S	sensitizing dye in a DSSC
τ_{em}	emission lifetime
TAC	time-to-amplitude converter
$TBAPF_6$	tetrabuytlammoniumhexaflourophospate
TCSPC	time correlation single photon counting
THF	tetrahydrofuran
Voc	open circuit photovoltage

CHAPTER 1.

GROUND-STATE ASSOCIATION BETWEEN PHENOTHIAZINE AND TRIS(DIIMINE)RUTHENIUM(II) COMPLEXES: ITS ROLE IN HIGHLY EFFICIENT PHOTOINDUCED CHARGE SEPARATION

NOTE: This chapter consists of material that has been published as a full paper in the Journal of the American Chemical Society (Weber, J.M.; Rawls, M.T.; MacKenzie, V.J.; Limoges, B.R.; Elliott, C.M. "High Energy and Quantum Efficiency in Photoinduced Charge Separation" J. Amer. Chem Soc. 129, 313-320 (2007)). The text of the chapter has been modified from the publication in order to incorporate additional data and information into the chapter. The contributions of the other authors to this work are summarized as follows: V.J. MacKenzie was responsible for building the nanosecond laser spectrometer; B.R. Limoges provided Figure 4 and performed the 2-D NMR experiments showing evidence of intramolecular donor-chromophore interactions which appear in the supplemental material section at the end of the chapter; M.T. Rawls' work also appears in the supplemental material section. Otherwise, the experimental work presented is mine. The data interpretation was a collaborative effort between me and my advisor, Professor C.M. Elliott.

Introduction

Numerous synthetic molecular systems exist that can effect photoinduced charge separation. Several reviews of this general area have appeared, some of which are quite recent and contain hundreds of specific references[1-4]. These reviews and the references they contain can be consulted for an overview of the area. The types of assemblies that have been studied vary widely in structure, complexity and the molecular components they incorporate[1-4]. Additionally, there is a significant variance in the efficiency with which charge separation can be achieved and in the lifetime of the resultant charge separated state (CSS).

A significant portion of the effort in this area has focused on so-called "triad" assemblies incorporating an electron acceptor (A), an electron donor (D) and a light absorbing chromophore (C). The components of these triads typically consist of a central trisbipyridine ruthenium(II) chromophore ($RuL_3^{2+} = C^{2+}$) covalently linked to one or more phenothiazine donors (PTZ = D) and to an N,N'-diquaternary-2,2'-bipyridinium electron acceptor ($DQ^{2+} = A^{2+}$)[5-8]. The linkages between the chromophore and the D and A^{2+} moieties are typically polymethylene chains emanating from the periphery of bipyridine ligands. Thus, the saturated alkyl chains bridging the molecular components are both nominally electrically insulating and flexible. The molecule shown in Figure 1 is a typical example of such a triad assembly [5-8].

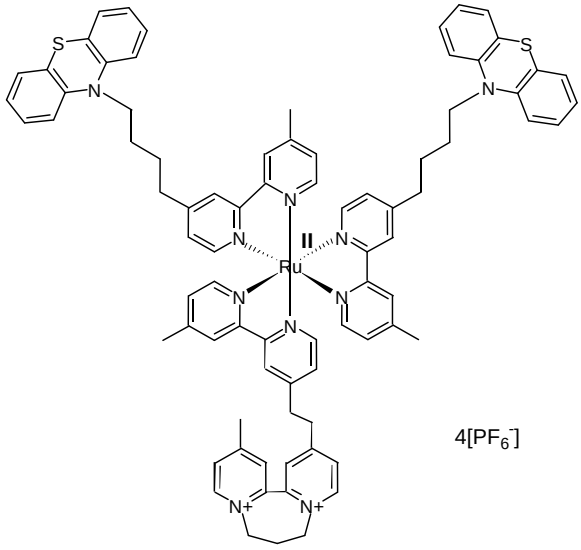

Figure 1-1. A Donor-Chromophore-Acceptor triad complex that separates charge with near unity quantum efficiency.

Considering the many types of light-induced charge-separation systems that exist, there is no *a priori* reason one should expect triads such as in Figure 1 to be unusually efficient at charge separation; yet, they are. Typically, D-C^{2+}-A^{2+} systems of this type undergo photoinduced CSS formation with very high efficiencies, often approaching unity[9,10]. Additionally, counter to what Marcus Theory predicts, there seems to be little correlation between the thermodynamic driving force for the various electron transfer steps and Φ_{CSS}. To illustrate this point, the CSS formed from D-C^{2+}-A^{2+} triad in Figure 1 stores ca. 1.33 eV of energy—an amount equal to about 66% of the ^{3}MLCT energy and 50% of the incident photon energy at λ_{max} of the chromophore absorption (460 nm). Altering the diquat acceptor such that a four carbon chain links the two quaternary nitrogens, increases the energy stored in the CSS to 1.47 eV or 72% ^{3}MLCT energy and 55% of the incident photon energy at λ_{max}, yet both systems have essentially the same Φ_{CSS} (close to unity). Natural photosynthesis, on the other hand, has a theoretical maximum efficiency of

approximately 13% in converting photosynthetically active solar radiation (i.e., 400-720 nm) into chemically stored energy[11]. Natural photosynthesis does have an important advantage, however--the energy is stored essentially indefinitely. In these CSS, without additional charge separation steps, the energy can be stored only for a little more than a μs. Over the course of our studies with these D-C^{2+}-A^{2+} triads and analogous D-C^{2+} and C^{2+}-A^{2+} diads, a feature atypical of other functionally similar systems became evident—namely, indications of a ground-state intramolecular association between the RuL_3 chromophore and the phenothiazine donor[8,12,13]. These previous studies provided no proof that this apparent D/C^{2+} association is involved in the CSS formation. The form of the chromophore which is responsible for forming the CSS is a triplet metal-to-ligand charge-transfer excited state (^{3}MLCT) that is highly luminescent in the absence of any attached acceptors or donors. The solution emission lifetime (ε_{em}) is ca. 600 to 900 ns dependent upon the solvent. Diad assemblies of both C^{2+}-A^{2+} and C^{2+}-D have been prepared and their emission lifetimes examined in order to establish the respective quenching rates. As the driving force is changed and numbers of methylenes in the chain linking C^{2+} and A^{2+} are varied from 2 to 6, the oxidative electron transfer quenching rates for C^{2+}-A^{2+} diads vary from about 1 X 10^{10} to 1 X 10^7 s^{-1} [6,8,14-16]. In contrast, as the numbers of methylenes in the chain linking C^{2+} and D is varied from 1 to 9, the reductive quenching rates for C^{2+}-D vary only from ca. 5 X 10^6 to 1 X 10^6 s^{-1} in 1,2-dichloroethane solvent [7,12]. Thus, the slowest oxidative quenching is at least 50 times faster than the fastest reductive quenching. More importantly, when the emission decay rate of *any* D-C^{2+}-A^{2+} triad is compared with that of the corresponding C^{2+}-A^{2+} diad (i.e., with the same A^{2+}-containing ligand), the *relative rates* never differ by more than a factor of two even though the absolute decay rates change by over a factor of ca. x 10^3.

The conclusion that must be drawn from these data is that the initial quenching event in all D-C^{2+}-A^{2+} triads of this family is *always* oxidative quenching and D is, at this point, not involved:

$$D\text{-}C^{2+*}\text{-}A^{2+} \rightarrow D\text{-}C^{3+}\text{-}A^{+\bullet}$$

Another relevant fact from these earlier studies is that, in the time-resolved absorption spectra of the C^{2+}-A^{2+} diads, there is never any evidence of $A^{+\bullet}$ being present[6]. One must conclude then, that the back electron transfer rate for

$$C^{3+}\text{-}A^{+\bullet} \rightarrow C^{2+}\text{-}A^{2+}$$

must be significantly faster than the oxidative quenching rate.

At this juncture, the stage has been set to propose two alternate hypotheses for the origin of the abnormally large Φ_{CSS} values of these triads:

1. The rate of intramolecular electron transfer between D and C^{3+} is inherently and significantly faster than between C^{3+} and $A^{+\bullet}$ and there is nothing else unusual about these triads.
2. The rate of intramolecular electron transfer between D and C^{3+} is abnormally fast as a result of some type of ground-state association involving D prior to photoexcitation.

In order to test these hypotheses it is necessary to determine the effect on Φ_{CSS} of varying the relative concentrations of D and C. Obviously, this cannot be done in an entirely intramolecular system. In the present study we provide both additional evidence for the D/C^{2+} association and evidence that it is intimately involved in CSS formation. However, the way the D/C^{2+} association is involved is counter-intuitive. As will be demonstrated, the initial electron-transfer *does not* directly involve the donor. *Irrespective of the presence or absence of the donor, the photo-excited chromophore is quenched oxidatively by the attached acceptor.* It is only after this initial electron transfer from the excited chromophore to the acceptor that the

donor/chromophore association becomes important; and it does so by promoting the rapid reduction of the oxidized chromophore prior to geminate C^{3+}-$A^{+\bullet}$ recombination (as depicted in Scheme 1).

Herein are reported studies on the light-induced charge separation occurring between *bimolecular* analogs of D-C^{2+}-A^{2+} triads represented in Figure 1 - specifically between a C^{2+}-A^{2+} diad and a PTZ-type donor, D. By employing a two-component system, it is possible to systematically study the chromophore/donor association equilibrium. Finally, these studies provide an explanation for the unusually high quantum efficiencies observed for related D-C^{2+}-A^{2+} triad assemblies.

Scheme 1. A depiction of the phenothiazine electron donor moeity associating with the local bipyridine ligand in a triad assembly such as in Figure 1.

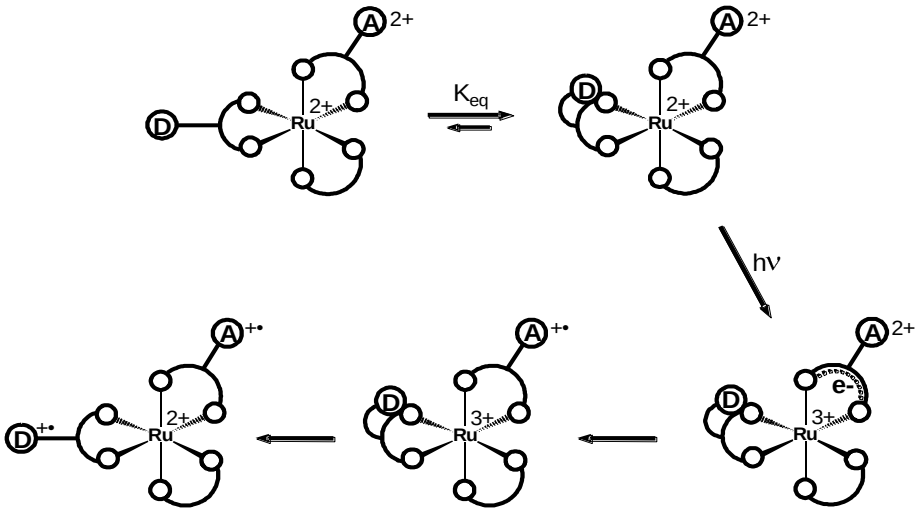

Figure 2 shows the C^{2+}-A^{2+} moiety, **VI**, chosen for the present study. The C^{2+} and A^{2+} components differ somewhat from those comprising the D-C^{2+}-A^{2+} assemblies represented in

Figure 1. First, the electron acceptor is a "paraquat-type" moiety rather than a "diquat" (i.e., it is based on a N,N'-dialkyl-4,4'-bipyridinium instead of an N,N'-dialkyl-2,2'-bipyridinium)[17]. Second, the two "remote" ligands on the ruthenium (i.e., the ones not having an appended paraquat) are 1,10-phenanthroline rather than 2,2'-bipyridine. The interaction responsible for the C^{2+}/D associations is most likelyππ in nature (*vide infra*); thus, we surmised that the more extended π system afforded by phenanthroline might enhance the association. Moreover, from the ruthenium's perspective, the electronic difference between phenanthroline and bipyridine are fairly minor (i.e., $Ru(bpy)_3^{2+}$ and $Ru(phen)_3^{2+}$ have very similar visible spectra and redox properties)[18]. The choice of paraquat acceptor was made based on the recombination kinetics of the initial electron-transfer quenching product of the bipyridine analog of **VI** [14,17] . Irrespective of whether the acceptor is a diquat or a paraquat, the initial electron-transfer event following photo-excitation is the donation of an electron from the ^{3}MLCT excited state of the RuL_3^{2+} to the acceptor[8,15,16]. In the absence of a donor, the back electron transfer rapidly ensues. For all C^{2+}-A^{2+} diads based on diquat-type acceptors, that rate is significantly faster than the forward rate; thus, only a lower limit for its rate constant, k_{bet}, can be established[6]. In contrast, Mallouk et al. were able to measure the recombination rate of $[Ru^{III}(bpy)_2(bpy\text{-}PQ^{+\bullet})]$ where $bpy\text{-}PQ^{+2}$ is the same acceptor ligand as in **VI** (see Figure 2)[19]. For these reasons, the C^{2+}-A^{2+} diad, **VI**, shown in Figure 2 was employed in the present study.

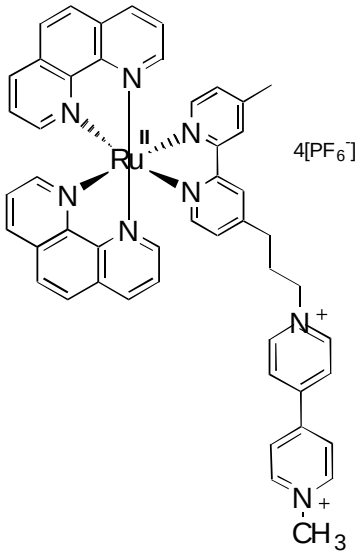

Figure 1-2. The C^{2+}-A^{2+} diad, **VI**, used in bimolecular experiments with N-MePTZ donor.

The choice of donor was straightforward. The redox potentials of N-alkylphenothiazines are essentially insensitive to the identity of the alkyl group. A methyl group is the least sterically demanding alkyl substituent possible, so N-methylphenothiazine (N-MePTZ) was employed.

Experimental

Syntheses

Unless otherwise stated, all chemicals were obtained from Aldrich and used without further purification. Solvents (Fisher) were ACS Grade and used as received. 4,4'-Dimethyl-2,2'-bipyridine (DMB) was purchased from Reilley Industries, Indianapolis and recrystalized from ethyl acetate. Lithium diisopropylamid (LDA) was prepared by the addition of a heptane solution of n-butyllithium to diisopropylamine in tetrahydrofuran (THF). Acetonitrile solvent for spectroscopy applications was Fisher Optima Grade. THF was dried and freshly distilled prior to each use by refluxing under nitrogen over sodium/benzophenone.

4-(3-hydroxypropyl)-4'-methyl-2,2'-bipyridine, (I). Under nitrogen, 0.95 equivalents of LDA in THF was added to 10.0g of 4,4'-dimethyl-2,2'-bipyridine (DMB) which had been dissolved in 200 mL of THF and cooled to –78 °C. This solution was stirred for 3 hours. A 4-fold excess of ethylene oxide was then added via cannula. The reaction mixture was allowed to warm to room temperature and stirred for 18 hours before quenching by addition of 100 mL of water. The THF was removed by rotary evaporation and the product, 4-(3-hydroxypropyl)-4'-methyl-2,2'-bipyridine, was extracted into methylene chloride (100 mL;3X) from the aqueous slurry. The methylene chloride fractions were combined and brought to dryness by rotary evaporation. The solid residue was redissolved in ca. 150 mL of ethyl acetate and cooled to 0 °C whereupon much of the unreacted DMB precipitated from solution while the product remained dissolved. Ethyl acetate was removed by rotary evaporation at room temperature, yielding the product contaminated with DMB. This crude product was purified by "flash" silica gel chromatography, eluting first with 10% ethyl acetate in methylene chloride until all DMB was off of the column. The product was then eluted from the column by gradually increasing the mobile phase polarity by changing the ethyl acetate:methylene chloride ratio. After rotary evaporation of solvent, the remaining white solid, **I**, was vacuum-dried overnight to yield 5.1g of product (41%); ^{1}H NMR ($CDCl_3$) δ $-CH_2-$ 1.9 (quintet), CH_3 2.4 (s), $-CH_2-$ 2.8 (t), $-CH_2OH$ 3.7 (t), aromatic 7.2, 8.3, 8.6.

4-(3-Bromopropyl)-4'-methyl-2,2'-bipyridine, (II). 4-(3-hydroxypropyl)-4'-methyl-2,2'-bipyridine was converted to **II** by refluxing for 12 hours in a 1:1 mixture of aqueous HBr (48%) and acetic acid. The reaction mixture was cooled and the pH was brought into the range of 5-6 by addition of aqueous sodium bicarbonate. The product was extracted into methylene chloride, which was then dried over magnesium sulfate, and filtered. The solvent was removed by rotary

evaporation at room temperature, yielding a red oil (88%); ^{1}H NMR ($CDCl_3$) δ $–CH_2–$ 2.2 (quintet), CH_3 2.4 (s), $–CH_2–$ 2.8 (t), $–CH_2Br$ 3.4 (t), aromatic 7.2, 8.3, 8.6.

[1-Methyl-4,4'-bipyridinium](PF$_6$), (III). 4,4'-Bipyridine was stirred with a two-fold excess of iodomethane in ether for 24 hours in the dark. The resulting yellow precipitate, [1-methyl-4,4'-bipyridinium] iodide, was filtered and washed with cold ether. Dissolving the iodide salt in water and adding a saturated aqueous solution of ammonium hexafluorophosphate dropwise yielded the hexafluorophosphate salt as a white precipitate. The precipitate, **III**, was washed with cold water and vacuum dried (28%); ^{1}H NMR (CD_3CN) δ CH_3 4.4 (s), aromatic 7.8, 8.4, 8.8, 8.9.

[1-(3-(4'-Methyl-2,2'-bipyridin-4-yl)propyl)-1'-methyl-4,4'-bipyridinediium](PF$_6$)$_2$, (IV). 0.5g of 4-(3-bromopropyl)-4'-methyl-2,2'-bipyridine, **II**, and 3.3g (6eq.) of [1-methyl-4,4'-bipyridinium](PF$_6$), **III**, were refluxed in 150mL of butyronitrile under nitrogen, excluding light, for 24 hours. The yellow precipitate was metathesized to the hexafluorophosphate salt by the procedure described above. Yield of 0.54g(46%); ^{1}H NMR (CD_3CN) δ $–CH_2–$, CH_3 2.4 (quintet + s), $–CH_2–$ 2.9 (t), N^+CH_3 4.4 (s), N^+CH_2 4.7 (t), aromatic 7.2 - 8.9.

Ru(1,10-phenanthroline)$_2$Cl$_2$, (V). 1.0g of $Ru(DMSO)_4Cl_2$[20] was dissolved in 25 mL of dimethylformamide (DMF) which was previously dried over alumina. This solution was saturated with lithium chloride before adding 0.82g (2eq.) of 1,10-phenanthroline. The reaction mixture was warmed to just below reflux and stirred for one hour. Additional lithium chloride was then added and the temperature increased to full reflux. After 75 minutes of reflux, the solution was cooled to room temperature and 60mL of water added. The precipitated crude product, **V**, was filtered and vacuum-dried (17%) and used in subsequent reactions without further purification; ^{1}H NMR (CD_3CN) aromatic 7.1 - 8.7.

[Ru(1,10-phenanthroline)$_2$(4-(3-(1'-methyl-4,4'-bipyridinediium-1-yl)-propyl)-4'-methyl-2,2'-bipyridine)](PF$_6$)$_4$, (VI). 79mg of $Ru(phen)_2Cl_2$ and 100mg(1eq.) of [1-(3-(4'-methyl-2,2'-bipyridin-4-yl)propyl)-1'-methyl-4,4'-bipyrinediium]$(PF_6)_2$, **IV**, were refluxed in methanol for 18 hours. The reaction vessel was kept in the dark under nitrogen for the duration of the reaction. Upon cooling to room temperature, a precipitate formed which was filtered off and discarded. A solution of methanol saturated with ammonium hexafluorophosphate was added dropwise to precipitate the crude product, **VI**, as the hexafluorophosphate salt. "Flash" silica gel chromatography was used to isolate the product. The "full strength" elution solvent was 50:40:10 water/acetonitrile/ saturated aqueous KNO_3. A gradient elution with the mobile phase was required where the full strength elution solvent was diluted at each stage with 1:1 acetonitrile:water. The crude product was dissolved in neat acetonitrile and loaded on to approximately 5 inches of flash silica gel in a 1" diameter column. The column was first eluted with progressively less dilute solvent starting with a 20-fold dilution and ending with "full strength". Fractions containing only the desired product (as determined by TLC) were combined and the acetonitrile removed by rotary evaporation at just above room temperature. The product was metathesized to the hexafluorophosphate salt and the resulting precipitate washed with water. Yield of 66mg(30%); ^{1}H NMR (CD_3CN) δ $-CH_2-$ 2.4 (quintet), CH_3 2.5 (s), $-CH_2-$ 2.9 (t), N^+CH_3 4.4 (s), N^+CH_2 4.7 (t), aromatic 7.1 - 8.9; GC/MS (ES^+) *m/z* calcd. 1279.15, found 1279.00.

[Ru(1,10-phenanthroline)$_2$(4,4'-dimethyl-2,2'-bipyridine)](PF$_6$)$_2$, (VII). 100 mg of **V** and 34 mg of DMB were dissolved in 25 mL of ethanol and brought to reflux for 20 hours. 15 ml of ethanol were removed by rotary evaporation before 30mL of water were added. The product was metathesized to the hexafluorophosphate salt as described and recrystallized twice from

methanol. Yield of 26 mg(25%); ^{1}H NMR (CD_3CN) δ CH_3 2.5 (s), aromatic 7.1 – 8.7; GC/MS (ES^+) *m/z* calcd. 791.14, found 791.07.

Preparation of Samples

Sample solutions were prepared in a dark room and kept from light until frozen for degassing. A stock solution of **VI** in dichloromethane (Aldrich – Spectro Grade) was prepared by adding solvent to a small amount of the solid complex until the absorbance at the maximum of the MLCT band monitored at 450nm in a 1 cm cell was approximately 0.15 (ca. 10^{-5}M). The appropriate amount of solid N-MePTZ to obtain each concentration desired was weighed into vials and 3mL of stock solution of **VI** added to each vial. Samples were then transferred to an optical cell constructed with a side-arm for freeze-pump-thaw (FPT) degassing, a teflon valve, and a fitting for attachment to a vacuum line. Solution in the cell was transferred to the sidearm and frozen in liquid nitrogen. Each sample was FPT degassed several times until there was no evidence of outgassing upon thawing.

Transient Absorption Measurements

The initial amount of charge-separated state formed was determined by transient absorption spectroscopy. The 355nm tripled output of a Spectra-Physics Lab-190 Nd:YAG laser producing 8ns pulses at 30Hz with a power of approximately 2.0W was used to pump Coumarin 450 dye in a Spectra-Physics PDL-3 dye laser. The dye laser output at 450nm was used to excite the sample. Typical output powers were approximately 70mW. An Oriel 75W Xenon arc lamp was employed as a continuous probe source.

The reduced viologen acceptor radical has an absorbance maximum at 397 nm. This wavelength was isolated from the Xenon lamp's continuous output using a Johnson and Johnson monochromator. Subsequent to passing through the sample cell, the probe beam was collimated

and then focused onto the entrance slit of a Jarrell Ash model 82-410 monochromator after passing through a mechanical chopper operated at 30 Hz with slits such that light was transmitted only about 3% of the time. The photodiode output from the chopper was used as the trigger signal for the Nd:YAG laser. A Hamamatsu model R2496 photomultiplier tube (PMT) was employed to monitor the intensity of the probe beam. A Tektronix TDS 620B digital oscilloscope recorded the current output from the PMT for the first 500ns following excitation by the pump beam. The oscilloscope was triggered with a Thorlabs DET210 fast photodiode. The results from 200 pulses were averaged. Differential absorbance due to the reduced viologen acceptor was calculated using Beer's Law.

Emission Lifetime Measurements

Emission lifetimes of **VI** in dichloromethane were obtained employing time correlation single-photon counting (TCSPC) as described by O'Connor and Phillips[21]. A Ti:sapphire regenerative amplifier (Coherent RegA) produced pulses centered at 866 nm with a 200 kHz repetition rate and 650 μJ/pulse. The light was frequency doubled to promote the MLCT transition. The subsequent fluorescence relaxation was collected through a subtractive double monochromator. Single photons impinging on a microchannel plate detector (Hamamatsu, MCP-PMT) were detected and digitized using an analog-to-digital converter (Oxford ADC) and served as the start pulse for a time-to-amplitude converter (Oxford TAC). A small fraction of the excitation light was split off and directed to a fast photodiode (ThorLabs). This served as the stop pulse for the TAC. Signals from the TAC were fed into a multichannel analyzer (Oxford MCA) whose output was monitored by a computer. Decay traces were collected until sufficient signal-to-noise was achieved to allow adequate data analysis.

Solution Viscosity Determination

Solution viscosities were measured using Ostwald – type viscometers from Cannon Instrument Co.

Results

Evidence for a Donor/Chromophore Interaction in the Ground State

Our first indication of an intramolecular RuL_3/PTZ ground-state interaction came from early spectral work with D-C^{2+}-A^{2+} triads, and C^{2+}-A^{2+} and D-C^{2+} diads[6-8,12]. Within experimental error, the visible spectrum of a given C^{2+}-A^{2+} diad can be exactly reproduced by simply summing the correctly weighted spectra of the individual components (i.e. of A^{2+} and C^{2+}). In contrast, whenever a covalently bound PTZ donor is present (i.e. for D-C^{2+}-A^{2+} or D-C^{2+} species) this is not possible. There is always a slight difference between the calculated and authentic spectra. The difference is manifest most notably as a modest broadening of the MLCT absorption-band, for D-C^{2+}-A^{2+} and D-C^{2+} relative to C^{2+} [7,12]. Attempts to use visible spectroscopy to quantify the intermolecular interaction between N-MePTZ and either $Ru(bpy)_3^{2+}$ or $Ru(phen)_3^{2+}$ have been unsuccessful because of overlap from the intense MLCT transitions[9]; nevertheless, the qualitative effect of added N-MePTZ on the MLCT band of **VII** can be clearly seen from the spectra in Figure 3.

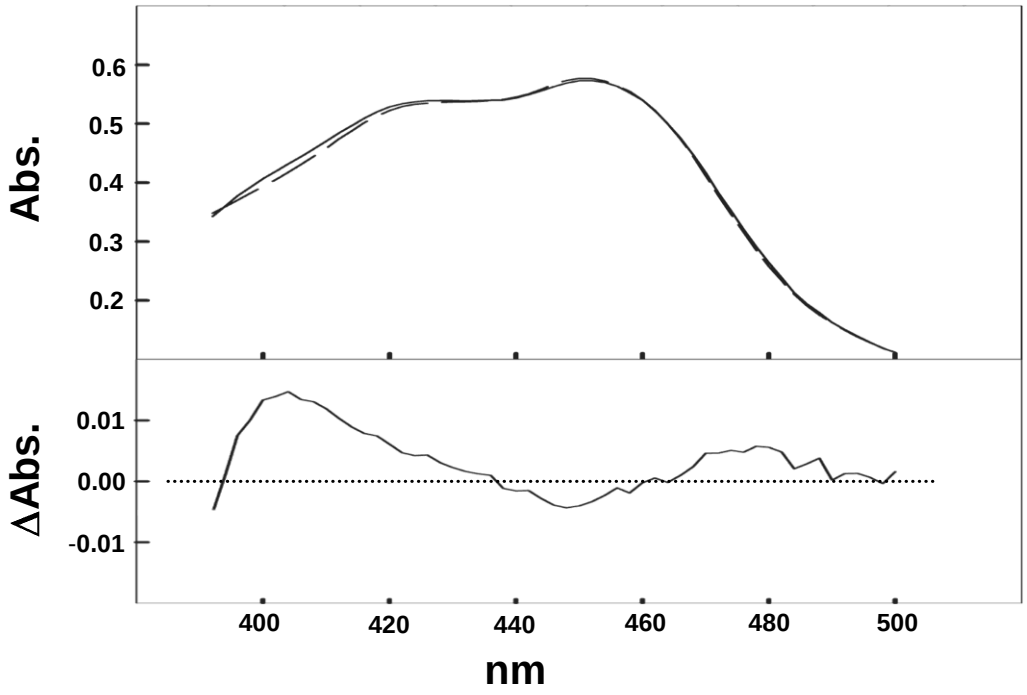

Figure 1-3. Visible spectra of a ca. 3×10^{-5} M solution of **VII** in dichloromethane (solid curve) and the same solution containing 50 mM N-MePTZ (dashed curve). The spectrum from the N-MePTZ-containing solution has been corrected by subtraction of the spectrum of a 50 mM N-MePTZ solution in dichloromethane. The lower part of the figure is the difference spectrum obtained from the solid and the dashed spectra.

In contrast to $Ru(L)_3^{2+}$ complexes, the analogous interaction between N-MePTZ and $Zn(phen)_3^{2+}$ is easily and directly observable since $Zn(phen)_3^{2+}$ lacks visible absorption above ca. 340 nm. Figure 4 shows the spectrum of a ca. 0.1 M solution of N-MePTZ, a spectrum of ca. 0.1 M solution of $[Zn(phen)_3^{2+}]$ $(ClO_4^-)_2$ and the spectrum of the same two solutions combined in equal amounts. In the figure the spectra of the two individual components (i.e., Figure 4a and b) have been scaled by ×0.5 to account for dilution and allow for quantitative comparison with the

mixed solution (Figure 4c). The combined solution has an absorbance absent from the other solutions that is clearly visible to the eye. Neither individual solution has any perceptible color but the combined solution is distinctly yellow. Moreover, concentrating the solution by evaporating the solvent, intensifies the yellow color until finally leaving a bright yellow film on the walls of the flask. While the metal-based redox properties of $Ru(phen)_3^{2+}$ and $Zn(phen)_3^{2+}$ are vastly different, their structure, charge and *ligand-based* redox properties are quite similar; thus it is reasonable that a similar association with N-MePTZ would exist (since the association likely involves simple van der Waals type π-π interaction and possibly some partial charge-donation from the PTZ to a phenanthroline).

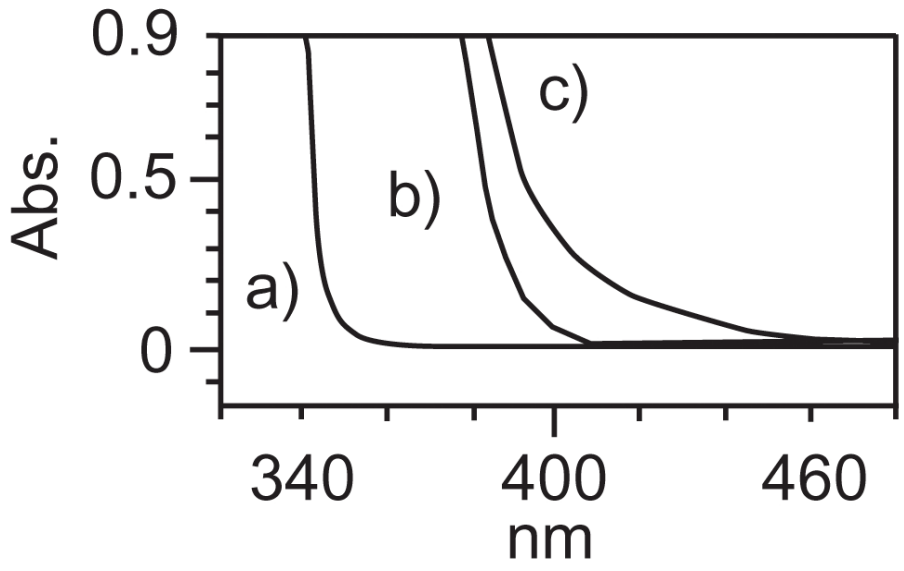

Figure 1-4. UV/Vis spectra of a) 0.1 M $Zn(phen)_3^{2+}$, b) 0.1 M N-MePTZ, and c) N-MePTZ + $Zn(phen)_3^{2+}$ in acetonitrile. Spectra a) and b) have been scaled by ×0.5 to account for dilution.

Bimolecular Photoinduced Charge Separation

Before discussing results on bimolecular CSS formation, it is useful to consider emission lifetime data for **VI** and **VII.** Recall that these complexes differ only in that **VII** lacks the appended paraquat electron acceptor**.** In degassed dichloromethane solvent the excited-state lifetime of **VII** is 410 ns at room temperature. Upon the addition of 10 mM N-MePTZ to the solution, the emission lifetime decreases to 64 ns as a result of *reductive quenching* of the ^{3}MLCT state by N-MePTZ. From the standard Stern-Volmer treatment, the bimolecular reductive quenching rate constant obtained is 1.32×10^9 $M^{-1}s^{-1}$. Using this value, the rate of bimolecular *reductive quenching* of **VI** by N-MePTZ can be calculated at any donor concentration. Considering the highest N-MePTZ concentration employed in this study, *the reductive quenching rate is calculated to be ×10 slower than the intramolecular oxidative quenching rate* determined from the emission lifetime of **VI** in the absence of any donor (vide infra). Consequently, it follows that *intramolecular oxidative quenching* by the paraquat electron acceptor is *always* the first step in the photoinduced electron transfer cascade for diad **VI** *irrespective of the presence or absence of N-MePTZ***.**

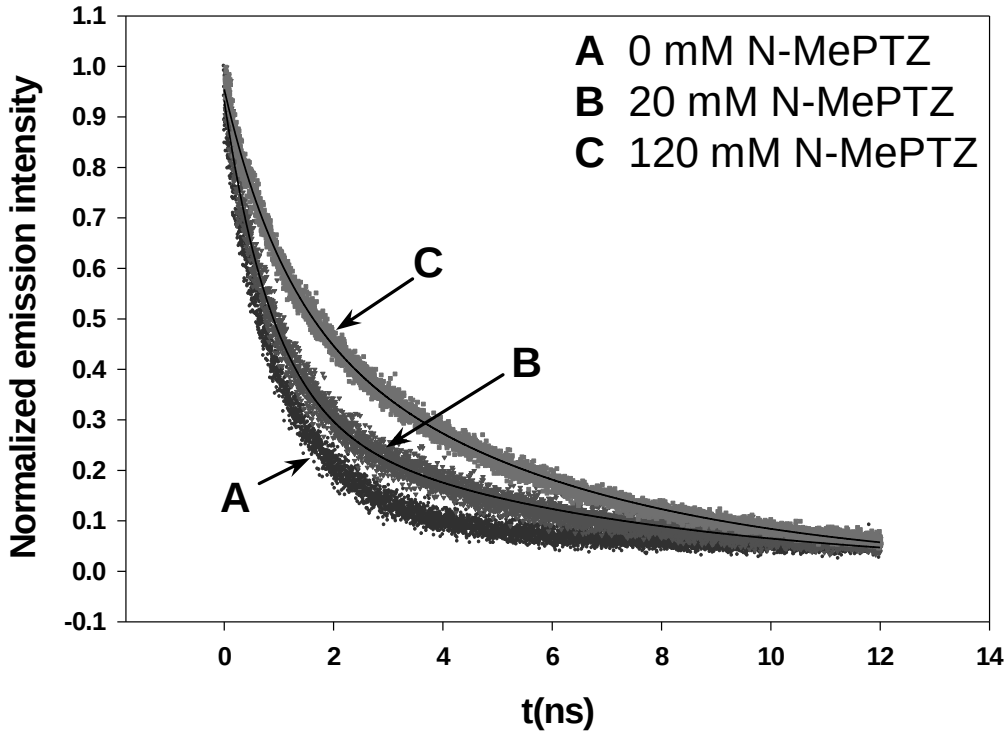

Figure 1-5. Time-resolved emission decays for a ca. 1×10^{-5} M solution of **VI** in oxygen-free dichloromethane: **A**, [N-MePTZ.] = 0.0 mM; **B**, [N-MePTZ.] = 20.0 mM; **C**, [N-MePTZ.] = 120.0 mM.

Changes in emission behavior of the C^{2+}-A^{2+} diad, **VI**, upon addition of N-MePTZ to solution reinforce the above conclusions. Figure 5 shows the emission decay of a ca. 1×10^{-5} M dichloromethane solution of **VI** in the presence, respectively, of 0, 20 and 120 mM N-MePTZ. Obvious from the figure is the fact that addition of N-MePTZ *increases* the average emission lifetime. A more quantitative evaluation reveals that the emission decays for the two solutions containing N-MePTZ are distinctly biexponential. For curves B and C in Figure 5, the lifetimes of the two components are, within experimental error, the same—the slow lifetime component being 3.8±0.2 ns and the fast being 0.72±0.03 ns. While the lifetimes are the same, the relative

contributions of the two components to the total emission are different at the different N-MePTZ concentrations. The significance of these decay kinetics will be considered subsequently in the context of transient absorption data on CSS formation; however, we emphasize again that the addition of N-MePTZ to solutions of **VI** does not result in reductive quenching since this process is far too slow to compete with the intramolecular oxidative quenching by the paraquat acceptor.

Transient absorbance spectroscopy was utilized to monitor the absorbance (397 nm) of the reduced viologen radical ($A^{+\bullet}$) resulting upon photoexcitation (450 nm) of the C^{2+}-A^{2+} diad (Figure 2) in the presence of N-MePTZ. Any viologen radical formed that does not result in CSS formation (from the CT state in Scheme 2, vide infra) recombines with the oxidized chromophore within the time of the laser pulse and thus does not contribute to the observed initial change in absorbance at 397 nm. Only when the donor reduces the oxidized chromophore prior to geminate recombination is CSS observed. The lifetime of the bimolecular CSS is on the order of tens of microseconds. Therefore, the change in absorbance at $t \rightarrow 0$ is directly proportional to the amount of CSS initially formed.

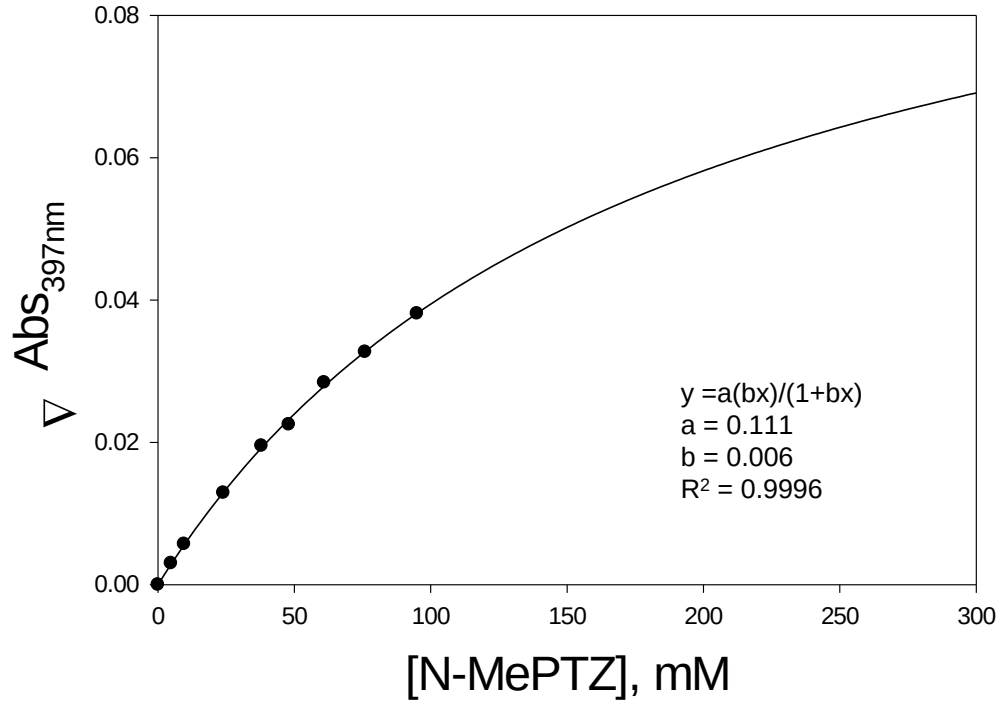

Figure 1-6. $\Delta A°_{397}$ (proportional to the amount of charge separated state initially formed) plotted vs. [N-MePTZ] in acetonitrile solvent.

The results obtained for CSS formation in acetonitrile solvent are shown in Figure 6. Concentrations of donor above 0.1M are not accessible because of solubility limitations. Also shown in the figure is the fit of the data to equation 3 (vide infra). While the range of [D] available in acetonitrile only permits about 40% of the predicted (from equation 3) range of $\Delta A°_{397}$ to be accessed, the quality of the fit is very good. The value of R^2 is 0.9996 which gives us considerable confidence that the data in Figure 6 truly follows the functional form expressed in equation 3 (vide infra). The same series of experiments was repeated using dichloromethane as the solvent. That data is shown in Figure 7. The solubility of N-MePTZ in dichloromethane is greater than in acetonitrile; moreover, it is possible to reach concentrations approaching those

yielding the limiting $\Delta A°_{397}$ value predicted from equation 3. As with acetonitrile, the fit at lower [D] to equation 3 is excellent but above ca. 20 mM there is some scatter. However, when only the data below 20 mM is used in the fit to equation 3, almost exactly the same values of *a* and *b* result as when the entire data set is used. Moreover, at the higher [D] there is moderate absorbance of N-MePTZ at 397 nm in dichloromethane which likely contributes to the scatter in $\Delta A°_{397}$. The fit indicates that the $\Delta A°_{397}$ at the highest concentration of N-MePTZ examined in dichloromethane ($\Delta A°_{397}$ ~ 0.032 at 100 mM) is much closer to the maximum limit predicted by the fit ($\Delta A°_{397,max}$ = 0.043) than was possible in acetonitrile.

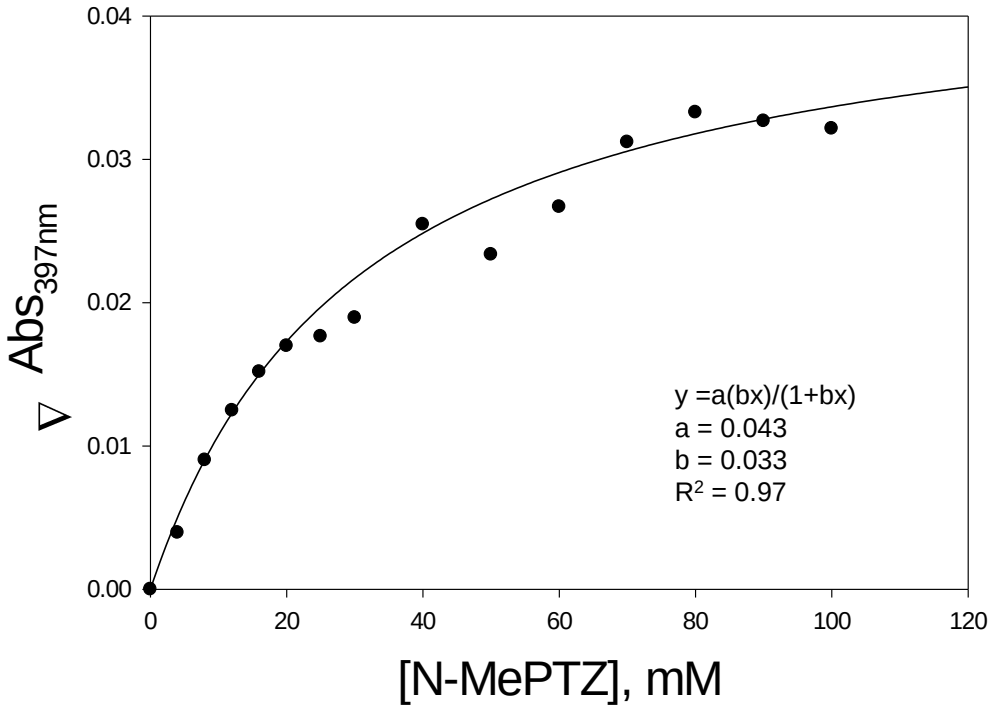

Figure 1-7. $\Delta A°_{397}$ (proportional to the amount of charge separated state initially formed) plotted vs. [N-MePTZ] in dichloromethane solvent.

Clearly obvious from Figures 6 and 7 is the fact that, at lower concentrations of donor, the initial amount of CSS formed is different for the two solvents at a given concentration of donor. To further probe the role of solvent, $\Delta A°_{397}$ was measured at a fixed [D] in binary mixtures of dichloromethane and acetonitrile and those results are presented in Figure 8. The relative amount of each solvent was varied from neat acetonitrile to neat dichloromethane. The concentration of N-MePTZ (20 mM) was chosen to give a large relative difference in $\Delta A°_{397}$ for the pure solvents but also such that enough CSS is produced in each solvent to be easily measured. Starting with neat acetonitrile, the amount of CSS formed remains roughly constant with increasing dichloromethane until the solvent is ca. 40% dichloromethane. Above that concentration, $\Delta A°_{397}$ increases roughly linearly up to the value obtained for pure dichloromethane.

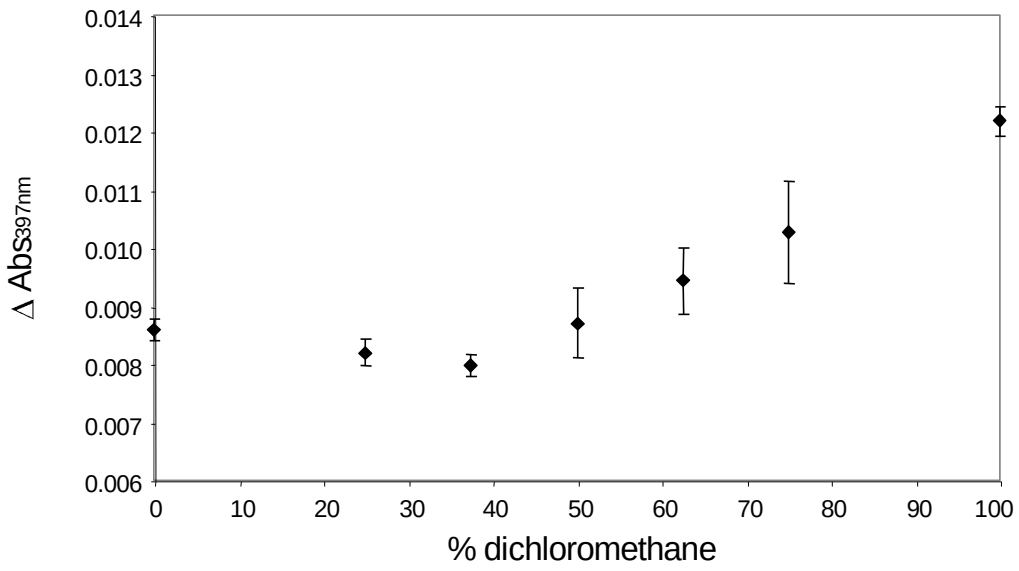

Figure 1-8. $\Delta A°_{397}$ (proportional to the amount of charge separated state initially formed) in the presence of 20 mM N-MePTZ plotted vs. % dichloromethane in a binary mixture of dichloromethane and acetonitrile.

Discussion

Represented in Scheme 2 are two limiting mechanisms for the reduction of the oxidized chromophore by the donor which lead to the CSS. As depicted in the left-hand branch of Scheme 2, after the initial oxidative quenching of the ^{3}MLCT state by A^{2+}, the donor, D, could simply diffuse through solution to the oxidized chromophore, C^{3+}, and reduce it via a collisional encounter. Alternatively, as represented in the right-hand branch of Scheme 2, prior to photoexcitation, the donor could already be associated with the complex. In this latter case, the effective concentration of donor and its electronic coupling to the chromophore are increased

(which would be expected to enhance the rate of electron transfer between the two). Within the constraints of these two models, quantitative relations can be derived expressing the initial concentration of CSS formed, $[CSS]_0$, as a function of donor concentration, [D].

Scheme 2. Jablonsky energy level diagram for analogous collisional (left-hand branch) and pre-association mechanisms (right-hand branch).

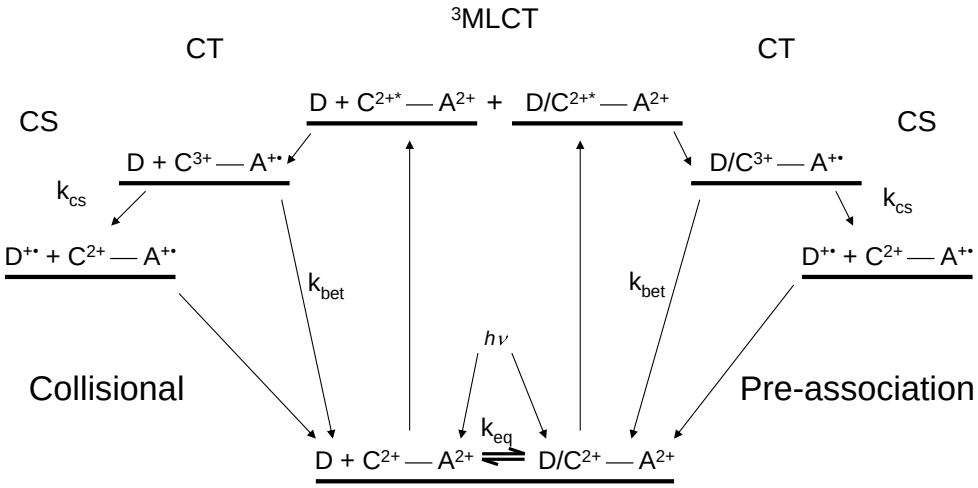

For the case of simple bi-molecular diffusional encounters between the N-MePTZ donor and C^{3+}-$A^{+\bullet}$ (i.e., left-hand side of Scheme 2), the resulting relationship takes the form:

$$\frac{[CSS]_0}{[CA]_i} = \frac{(k_{cs}/k_{bet})[D]}{1+(k_{cs}/k_{bet})[D]} \qquad (1)$$

where $[CA]_i$ is the total concentration of the C^{2+}-A^{2+} diad, k_{cs} is the bimolecular rate constant for forming the charge separated state and k_{bet} is the rate of geminate recombination between C^{3+}-$A^{+\bullet}$.

If, on the other hand, ground state association between the donor and metal complex were the appropriate mechanism responsible for CSS formation, the following relationship results:

$$\frac{[CSS]_0}{[CA]_i} = \frac{(k_{cs}/k_{bet})}{1+(k_{cs}/k_{bet})} \bullet \frac{K_{eq}[D]}{1+K_{eq}[D]} \qquad (2)$$

where K_{eq} is the complexation equilibrium constant. In deriving equation 2 it is assumed that an equilibrium association between the donor and chromophore is established prior to excitation and that CSS is only formed from that part of the total population of C^{2+}-A^{2+} that is associated with D in the ground state. Additionally, k_{bet} and k_{cs} are, respectively, first order rate constants of geminate recombination and charge separation relevant to the associated complex. In this instance k_{bet} may or may not be the same as k_{bet} in the absence of donor/chromophore association (i.e. as in equation 1).

In either of the above scenarios, the governing relation between $[CSS]_0$ and [D] has the same functional (i.e. mathematical) form. Additionally, since $[CSS]_0$ is directly proportional in either case to $\Delta A°_{397}$, the maximum change in absorbance at 397 nm after the excitation, both expressions can be written in the general form:

$$\Delta A°_{397} = a([D]/(b + [D])) \qquad (3)$$

In both cases the constant *a* depends on, among other things, experimental parameters such as the laser power and overlap of the pump and probe beams. For the sake of the work presented here, *a* can be considered to be an arbitrary constant in both models. In contrast, *b* is independent of similar experimental parameters (as long as they are constant). In the case of a simple bimolecular collisional reaction:

$$b = k_{bet}/k_{cs} \qquad (4)$$

In the case of equilibrium preassociation:

$$b = K_{eq}^{-1} \qquad (5)$$

As stated earlier, Mallouk et al. previously reported values for both k_{et} and k_{bet} obtained in acetonitrile for a C^{2+}-A^{2+} complex that differs from **VI** only in that the two phenanthroline ligands are replaced with bipyridines [19]. The forward electron-transfer rate constant, $k_{et,}$ for **VI** in dichloromethane (obtained from the emission decay in Figure 5) is 8.2×10^{10} s^{-1} which is fairly close to the value reported by Mallouk et al (1.9×10^{9} s^{-1}). It is reasonable to assume, therefore, that Mallouk et al's value of k_{bet} (6.5×10^{9} s^{-1}) is a reasonable lower-limit estimate for the analogous process in **VI**. Using this value and the value of *b* obtained from the fit to equation 3, a lower limit of 5.3×10^{10} $M^{-1}s^{-1}$ is obtained for k_{cs}. Using the standard relation[22],

$$k_{diff} = \frac{8RT}{3\eta} \qquad (6)$$

an estimate for the diffusion controlled limit for the rate of CSS formation in acetonitrile is calculated to be 2×10^{10} $M^{-1}s^{-1}$, where η is the viscosity of acetonitrile at room temperature. The lower limit for k_{cs} obtained from the fit to equation 3 is thus greater than the estimated diffusion controlled rate by a factor of ca. $\times2$.

Making the same assumptions and again using Mallouk's value for k_{bet}[19], a lower-limit value for k_{cs} of 2.2×10^{11} $M^{-1}s^{-1}$ is obtained from the dichloromethane results. From equation 6, the estimated diffusion-controlled rate is 1.7×10^{10} s^{-1}, which is more than an order of magnitude smaller than the bimolecular rate resulting from equations 3 and 4. Back electron-transfer rates for related compounds are typically not strongly solvent dependent; thus it is reasonable to conclude that, despite the difference in solvent, using Mallouk et al.'s value for k_{bet} as a lower-limit estimate is reasonable.[23-25] Furthermore, unlike Mallouk et al., we were unable to observe any photo-reduced acceptor with **VI** in the absence of N-MePTZ in either acetonitrile or dichloromethane. This fact reinforces the assumption that, in both solvents, $k_{bet} > 6.5 \times 10^{9}$ s^{-1} for **VI.**

The results above are strongly suggestive that the mechanism of CSS formation is not diffusional; however, a much stronger argument can be made by examining the dependence of Φ_{CSS} on solution viscosity. A series of stock solutions containing ca. 10^{-5} M C^{2+}-A^{2+} complex and 50mM N-MePTZ were prepared in dichloromethane solvent. To these solutions 0-80 mg/mL of polystyrene was added to increase solution viscosities. A corresponding weight of toluene was also added such that the (polystyrene + toluene):solvent ratio was held constant. The viscosity of each solution was measured five times and the averages ranged from 0.46cP to 12.1cP. Figure 9 shows the dependence of $\Delta A°_{397}$ on viscosity.

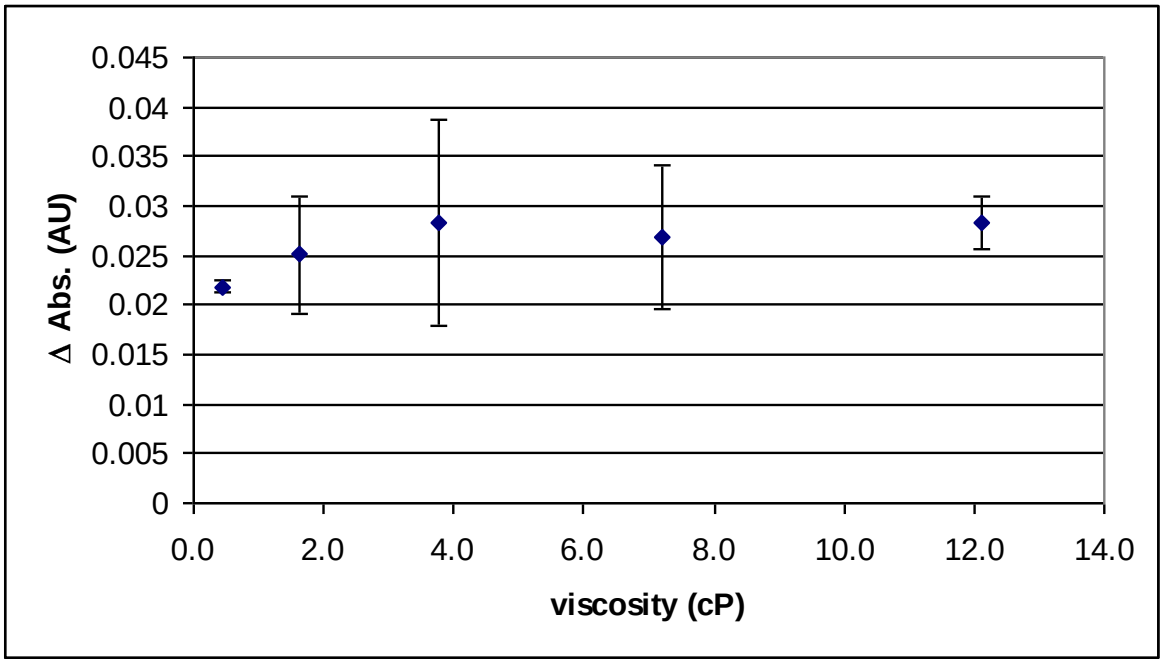

Figure 1-9. $\Delta A°_{397}$ (proportional to the amount of charge-separated state initially formed) in the presence of 50mM N-MePTZ plotted vs. solution viscosity. The error bars represent one standard deviation.

Finally, to unambiguously demonstrate that CSS formation by diffusional encounters between C^{3+} and D is not a reasonable possibility, one additional pair of solvent systems was considered. A stock solution containing ca. 10^{-5} M C^{2+}-A^{2+} complex and 50 mM N-MePTZ was prepared in dichloromethane solvent. Two identical aliquots of this solution were taken. Polystyrene was added to one solution and an equal weight of toluene was added to the other. The solution viscosities were measured and found to be, respectively, 18.5 cP and 0.44 cP. Upon photoexcitation, the $\Delta A°_{397}$ resulting from each of these two solutions was essentially identical—namely, 0.022 and 0.023. Clearly, a ca. 40-fold increase in viscosity with *no change* in $[CSS]_0$ effectively rules out any mechanism of CSS formation whereby simple collisional encounters between D and C^{3+}-$A^{+\bullet}$ are involved. By discrediting that mechanistic possibility, pre-association

between the donor and the chromophore complex in the ground state remains as the only viable mechanism for CSS formation.

It is appropriate at this point to compare the data of Figure 7 with the emission decay data of curves B and C in Figure 5. When the value of ΔA°_{397} from Figure 7 at any given [N-MePTZ] is divided by the predicted maximum ΔA°_{397} (0.043), the result is the fraction of CSS formed relative to the theoretical maximum CSS. Expressed as percentages, at 20 and 120 mM N-MePTZ one obtains values of 40% and 80%, respectively, from such a calculation. Recall that the lifetimes of the two components of the emission decay in curves B and C of Figure 5 are the same, only the relative contributions of the slow component changes. From the biexponential fits, the slow component contributes 45% and 70% to the total emission at 20 and 120 mM N-MePTZ, respectively. An interpretation of the close correspondence in these two sets of percentage values is that the slow component of the emission decay and the CSS formation arise from the same fraction of the C^{2+}-A^{2+} population—namely, the part that is in association with a N-MePTZ molecule at the instant of photoexcitation. The slower rate of electron transfer between C^{2+*} and A^{2+} when N-MePTZ is associated (resulting in the slow component of the emission decay) can be rationalized on the basis of sterics, thermodynamics or both. When the N-MePTZ is associated, the paraquat's intramolecular approach to the excited complex could be hindered, the reducing strength of the ^{3}MLCT state could be diminished or both.

Assuming an intramolecular version of the D/C^{2+} ground-state preassociation, Scheme 1 pictorially represents what would be operative in CSS formation for triads such as in Figure 1. Particularly significant is the fact that this mechanism provides an explanation for the unprecedentedly large quantum efficiencies of CSS formation observed across this class of D-C^{2+}-A^{2+} assemblies; but most importantly, it provides insight into a general means whereby

systems might be designed to give photoinduced charge separation with high quantum efficiencies.

Through numerous earlier studies with both C^{2+}-A^{2+} and D-C^{2+}-A^{2+} complexes, we have established that the quenching rate of the photoexcited chromophore changes by orders of magnitude with changes in A^{2+} [6,8,14-16]; in contrast, these rates are nearly insensitive to even the presence or absence of a D in the assembly[7,12]. Similarly, analysis of emission decay data for the bimolecular system examined here shows a very modest increase in the average excited state lifetime upon addition of N-MePTZ to solutions of **VI**. These results are entirely consistent with the mechanism portrayed in Scheme 1. The D/C interaction occurs but does not alter the fact that the ^{3}MLCT *reduces the attached acceptor in the initial step rather than oxidizing the D.* Such a mechanism is energetically reasonable as well. The driving force for reduction of the attached acceptor is favorable by at least 200 mV (depending on the specific acceptor present in the triad); whereas, oxidation of the donor by the ^{3}MLCT state is close to thermoneutral. Once the chromophore is oxidized, however, the driving force for oxidizing the PTZ is favorable by ca. 400 mV. In the absence of an attached donor there is no evidence of photoreduced diquat in any C^{2+}-A^{2+} analogs of the triads represented in Figure 1. Consequently, for the specific compound in Figure 1, the back electron transfer rate constant must be faster than about 10^{10} s^{-1} and the rate constant for oxidation of the donor must be at least 10^{11} s^{-1} to account for the CSS formation quantum efficiency (86±6 % observed in dichloroethane solvent) [9]. We have no direct evidence that donor/chromophore association is maintained once the chromophore is oxidized and prior to PTZ oxidation (i.e., the next to the last step of Scheme 2). It is reasonable however, to postulate that it is, given that any charge-transfer character in the D/C^{2+} interaction should be substantially enhanced in the D/C^{3+} species. One thing is virtually certain—once the PTZ is oxidized the

interaction will cease entirely and the complex should disassociate (for electrostatic reasons, if no other).

As stated earlier, the values of the constant *a* in equation 3 are dependent on the experimental conditions. Between experiments on the two solvent systems, these differed sufficiently to prevent drawing any conclusions from the *a* values. The constant *b* and the values of K_{eq} obtained therefrom are a different matter. Between dichloromethane and acetonitrile values of K_{eq} differ by approximately a factor of 5 (i.e., 33 vs. 6 M^{-1}, respectively). The non-linear dependence of K_{eq} on solvent composition shown in Figure 8 indicates the presence of specific solvent interactions in the equilibrium. The fact that the formation constant is smaller in acetonitrile might be rationalized on the basis of differences between solvation free energy of the chromophore in the two solvents. The cationic ruthenium complex should be more strongly solvated by acetonitrile. The process of forming the D/C^{2+} association likely disrupts the solvation sphere around both D and C^{2+} which should be, overall, energetically more costly in the more polar solvent.

Conclusion

The ground-state association between the phenothiazine donor and the ruthenium complex chromophore demonstrated herein plays a critical role in photoinduced CSS formation. By virtue of this association, orbital coupling between the D and C moieties is greatly enhanced such that the rate of electron transfer between the oxidized chromophore and the donor can efficiently compete with geminate recombination. Moreover, once the donor is oxidized the C^{2+} and $D^{+\bullet}$ dissociate, disrupting the strong coupling which otherwise would increase the rate of CSS decay. In other words, the electron-transfer process itself acts as a switch to turn off coupling along an undesirable pathway. Results from these bimolecular systems provide an

explanation for the unprecedented high quantum efficiency of CSS formation observed in the analogous triad systems. Considered in light of the present results, the triad assemblies provide the first example of which we are aware where a change in orbital coupling of this magnitude is induced by an intramolecular electron transfer. This suggests that related self-assembly processes could be intentionally designed and exploited to effect efficient CSS formation. Of particular importance is, in principle, that efficient photoinduced charge separation via such a mechanism should be possible without the loss in stored energy that almost inevitably accompanies efforts to use driving-force manipulations to improve CSS formation quantum efficiencies.

Supplemental Material

Effect of Acceptor on D Association

Figure SM1 is a plot analogous to Figure 3B except that the C^{2+}-A^{2+} had the paraquat acceptor replaced with the diquat acceptor shown in Figure 1. The C^{2+} portion of the molecule is identical to the chromophore in VI. The solid curve is NOT a fit to the data points in Figure SM1, rather it is the calculated line generated using the fit parameters obtained from the data in Figure 3B. The point of this figure is to demonstrate that the CSS formation (e.g., Keq) is NOT dependent upon the identity of A^{2+} in the C^{2+}-A^{2+} complex.

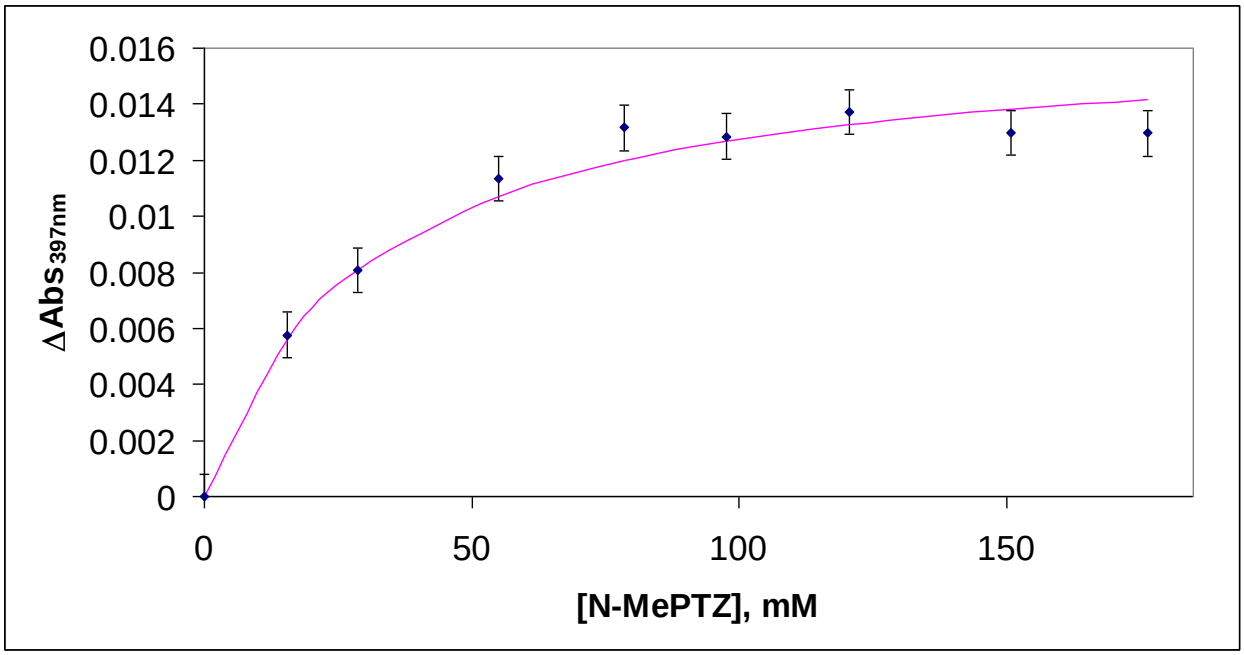

Figure SM 1. $\Delta A°_{397}$ for a CA with diquat acceptor in the presence of N-MePTZ in dichloromethane. The line was generated using the parameters from the CA viologen fit (from Figure 3B).

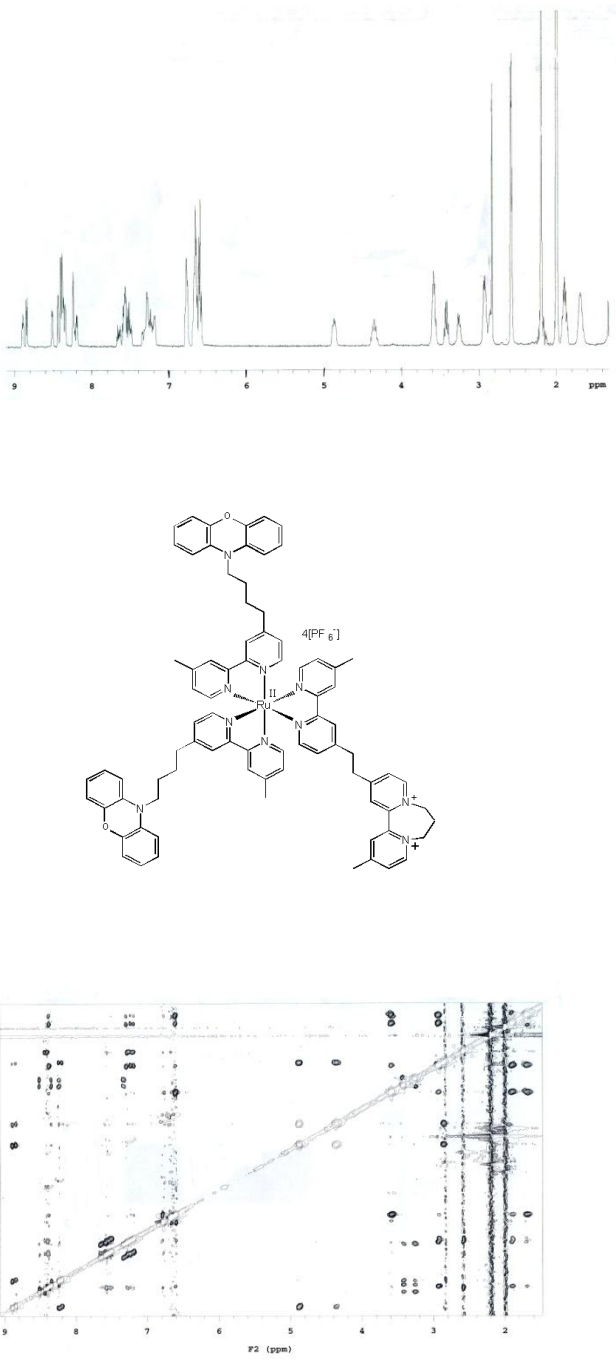

Figure SM 2. ^{1}H NMR and 2D Roesy NMR spectrum of covalently bound donor-chromophore-acceptor (structure shown upper right) triad in deuterated acetonitrile.

Examination of the spectrum shows conclusively that there are no correlations at all (significant within the limit of signal-to-noise) involving the diquat acceptor protons except those

with itself and with its linker methylene protons. There are, however, significant correlations between the bipyridine ligands (both ring and methyl protons) and the POZ donor protons.

Separation of the Oxidized Donor from the Association

ΔG = ~-9 kJ/mole for the D/C^{2+} association in dichloromethane (the solvent in which there is stronger association). If van der Waals interactions are responsible for the association, one might assume that the association free energy is independent of the oxidation state of either D or C. If one then treats the D^+ and C^{2+} as point charges at a distance of 40 pm in D^+/C^{2+}, the coulomb energy is about 80 kJ/mol, a factor of almost × 10 greater than what is necessary to overcome the van der Waals energy. Moreover, to whatever extent there is some small favorable component of charge transfer in the D/C^{2+} association, once the charge is transferred between C^{3+} and D, the association would be even less energetically favorable than if it were purely van der Waals in nature. It is, thus, fair to postulate that immediately after the electron transfer between C^{3+} and D, the D^+ and C^{2+} products would move away from each other at a rate somewhat greater than diffusion controlled (because of the electrostatic "push"). Finally, because back electron transfer between D^+ and C^{2+} is over 0.5 V up hill, the only electron transfer of importance at this point is between D^+ and A^+, for which we know the rate in the triad systems (ca. 7×10^6 s^{-1}).

ENDNOTES

(1) Kalyanasundaram, K. *Photochemistry of Polypyridine and Porphyrin Complexes*; Academic Press: San Diego, 1992.

(2) Schanze, K. S.; Walters, K. A. In *Organic and Inorganic Photochemistry*; Ramamurthy, V., Schanze, K. S., Eds.; Marcel Dekker: New York, 1998; Vol. 2, pp 75-127.

(3) Armaroli, N. *Photochem. Photobiol. Sci.* **2003**, *2*, 73-87.

(4) Scandola, F.; Chiorboli, C.; Indelli, M. T.; Rampi, M. T. In *Biological and Artificial Supermolecular Systems*; Wiley: Weinheim, 2003; Vol. 3, pp 337-403.

(5) Danielson, E.; Elliott, C. M.; Merkert, J. W.; Meyer, T. J. *J. Am. Chem. Soc.* **1987**, *109*, 2519-2520.

(6) Cooley, L. F.; Larson, S. L.; Elliott, C. M.; Kelley, D. F. *J. Phys. Chem.* **1991**, *95*, 10694-10700.

(7) Larson, S. L. Ph. D Dissertation, Colorado State University, 1994.

(8) Larson, S. L.; Elliott, C. M.; Kelley, D. F. *J. Phys. Chem.* **1995**, *99*, 6530-6539.

(9) Klumpp, T.; Linsenmann, M.; Larson, S. L.; Limoges, B. R.; Buerssner, D.; Krissinel, E. B.; Elliott, C. M.; Steiner, U. E. *J. Am. Chem. Soc.* **1999**, *121*, 1076-1087.

(10) Klumpp, T.; Linsenmann, M.; Larson, S. L.; Limoges, B. R.; Buerssner, D.; Krissinel, E. B.; Elliott, C. M.; Steiner, U. E. *J. Am. Chem. Soc.* **1999**, *121*, 4092.

(11) Bolton, J. R.; Hall, D. O. *Photochem. Photobiol.* **1991**, *53*, 545-548.

(12) Larson, S. L.; Elliott, C. M.; Kelley, D. F. *Inorg. Chem.* **1996**, *35*, 2070-2076.

(13) Limoges, B. Ph. D. Dissertation, Colorado State University, 2001.

(14) Schmehl, R. H.; Ryu, C. K.; Elliott, C. M.; Headford, C. L. E.; Ferrere, S. *Adv. Chem. Ser.* **1990**, *226*, 211-223.

(15) Cooley, L. F.; Headford, C. E. L.; Elliott, C. M.; Kelley, D. F. *J. Am. Chem. Soc.* **1988**, *1122*, 6673.

(16) Ryu, C. K.; Wang, R.; Schmehl, R. H.; Ferrere, S.; Ludwikow, M.; Merkert, J. W.; Headford, C. E. L.; Elliott, C. M. *J. Am. Chem. Soc.* **1992**, *114*, 430-438.

(17) Yonemoto, E. H.; Riley, R. L.; Kim, Y. I.; Atherton, S. J.; Schmehl, R. H.; Mallouk, T. E. *J. Am. Chem. Soc.* **1992**, *114*, 8081-8087.

(18) Balzani, V.; Juris, A.; Barigelletti, F.; Campagna, S.; Belser, P.; Von Zelewsky, A. *Coordination Chemistry Reviews* **1988**, *84*, 84-277.

(19) Yonemoto, E. H.; Saupe, G. B.; Schmehl, R. H.; Hubig, S. M.; Riley, R. L.; Iverson, B. L.; Mallouk, T. E. *J. Am. Chem. Soc.* **1994**, *116*, 4786-4795.

(20) Wilkinson, G.; Evans, I. P.; Spencer, A. *J. C. S. Dalton* **1973**, 204-209.

(21) O'Connor, D. V. P., D. *Time-Correlated Single-Photon Counting*; Academic Press: London, 1984.

(22) Atkins, P. W. *Physical Chemistry*; 5th ed.; W.H. Freeman and Co.: New York, 1994.

(23) Ohno, T.; Yoshimura, A.; Prasad, D. R.; Hoffman, M. Z. *Journal of Physical Chemistry* **1991**, *95*, 4723-4728.

(24) Sun, H.; Hoffman, M. Z. *Journal of Photochemistry and Photobiology, A: Chemistry* **1994**, *84*, 97-99.

(25) Linsenmann, M. Ph. D. Dissertation, Universtiy of Konstanz, 1997.

CHAPTER 2.

BACKGROUND AND SIGNIFICANCE OF ELECTRON TRANSFER MEDIATORS IN DYE-SENSITIZED SOLAR CELLS.

Photoelectrochemical cells employing photoanodes of nanocrystalline TiO_2 particles with light harvesting dyes adsorbed on their surface have been shown to have power efficiency conversions of ca.10 % when irradiated with direct sunlight.[1] This is a comparable efficiency to amorphous solid-state cells but falls well short of the efficiencies seen in single crystal silicon cells. Even though single crystal cells were developed decades ago their price has remained high. This is because, while silicon is the second most abundant element in the Earth's crust, silicon is found in its oxide form. While SiO_2 is cheap and readily available, the process for isolating electronic-grade silicon from its oxide is difficult and expensive. The extracted silicon must be ultrapure (99.999+ %) in order to grow a single crystal free of defects and adventitious dopants because such defects serve as traps for electrons which must be free to flow through the crystal in order to obtain efficient charge separation. In theory silicon solar cells could be around 33% efficient[2,3] but, because of reflection and other losses, operating efficiencies are typically around 22%. In dye-sensitized solar cells (DSSCs) only a single excited state participates in the absorption spectrum, so the efficiency is limited to 28.9%.[4] Because DSSCs offer the potential to construct high surface area cells out of relatively inexpensive materials, much effort has been devoted to understanding the fundamental principles of DSSC operation.[5] The resulting understanding has led to investigations of more efficient, robust and practical versions of DSSCs.

Figure 1 is a depiction of a DSSC. The current standard operating conditions are as follows: A photoanode consisting of a meso-porous film of nanocrystalline TiO_2 is deposited on SnO_2:F – coated glass and sintered in order for the TiO_2 to adhere to the glass and form a conducting pathway. The typical preparation follows the steps outlined by Huang, et al.[6] A sensitizing dye that absorbs light across a broad range of the solar spectrum is adsorbed on to the TiO_2 film. A metal chromophore, central to the sensitizing dye, is excited, promoting an electron from the metal center onto one of the bipyridine based ligands (see figure 2). The electron is then injected into the photoanode from the ligand based orbitals and subsequently is carried through a load to the cathode. The electron transfer mediator, iodide/triiodide (I^-/I_3^-), is reduced at the cathode and shuttles the electron back to the sensitizing dye which is then reduced back to its ground state. The typical cathode consists of a platinum film vapor deposited onto a conducting glass substrate. Methoxypropionitrile or similar solvent fills the cell and contains the I^-/I_3^- mediator system. The difference between the reduction potential of the mediator and the quasi-Fermi energy of the electrons in the photoanode conduction band determines the cell voltage.

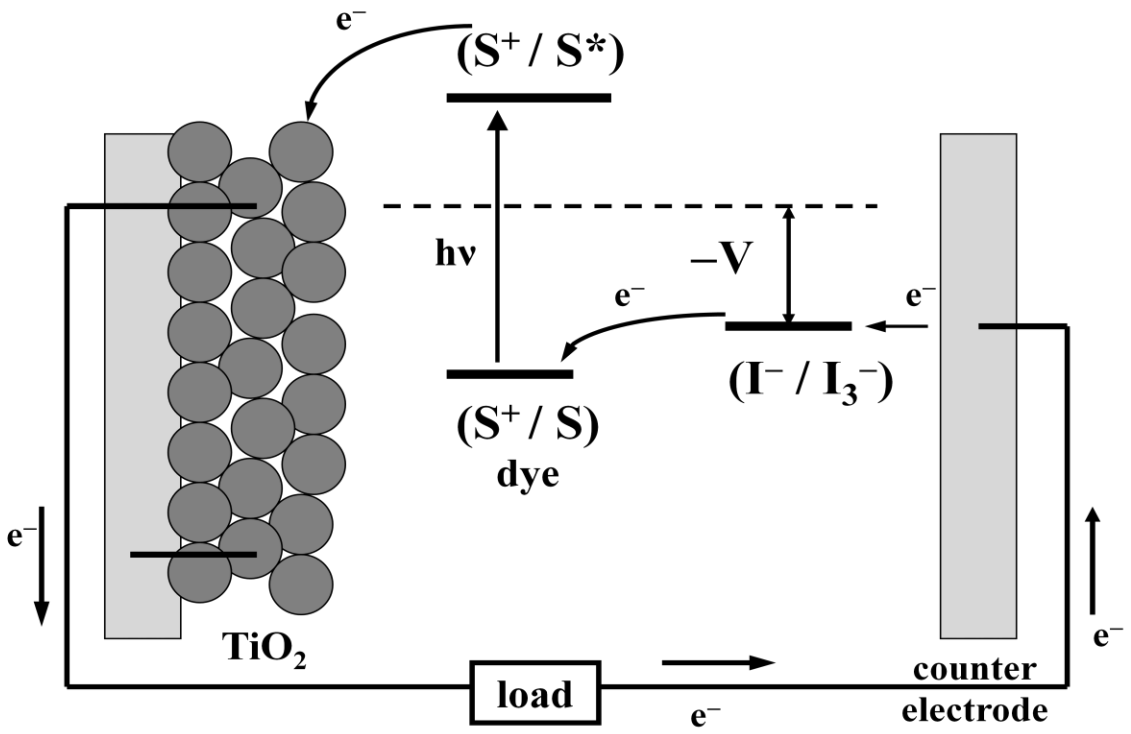

Figure 2-1. Schematic representation of the dye-sensitized photoelectrochemical cell.

While demonstrated energy efficiencies of DSSCs are comparable to existing commercial technologies, there are still several issues that must be addressed before DSSC technology could function as a viable commercial technology. The more important of these issues focus on the ruthenium based chromophore, the liquid-state electrolyte currently used to obtain the highest efficiencies and the limited set of electron-transfer mediators that will meet the cell kinetic requirements while also being compatible with the liquid-state electrolyte.

The best dyes to date for electron injection into the TiO_2 photoanode are ruthenium based chromophore complexes. Ruthenium is relatively rare and therefore expensive. Its ores are found in regions of the world that have historically been politically unstable. These issues pose serious questions about the long term cost effectiveness and availability of ruthenium as a central component in solar energy applications. The sensitizing dye most commonly used is cis-

diisothiocyanatobis(2, 2' – bipyridine-4,4'-dicarboxylic acid) ruthenium(II), referred to as the "N3" dye.[7] Figure 2 shows the structure of the N3 dye and its method of adsorption on the TiO_2 surface. Efforts have been made to find new dyes and to replace the liquid-state electrolyte.[8-12] However, efforts to replace the I^-/I_3^- electron-transfer mediator with other appropriate mediators have been modest because of the specific requirements that the sacrificial mediator must meet.[13-16] The focus of our research group in general and my research in particular has been to find new electron transfer mediators.

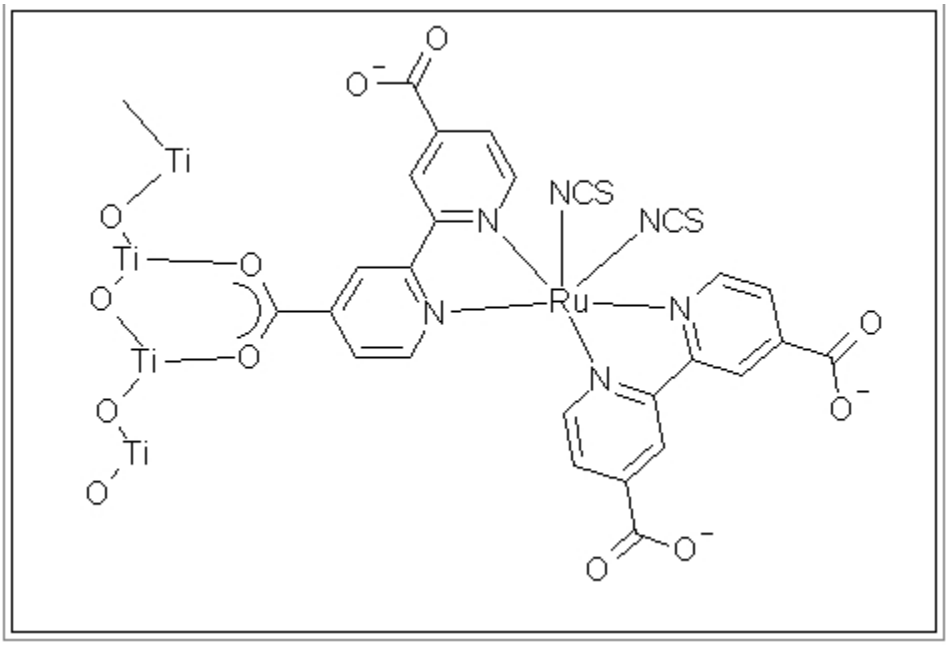

Figure 2-2. N3 dye adsorbed onto a TiO_2 surface. Figure reproduced from Hupp, et al.[17]

Before discussing possible alternatives to the I^-/I_3^-couple it is important to point out why this couple functions well and why the options to replace the couple are limited. In order to function as an effective mediator the reduction/oxidation (redox) couple employed must satisfy the kinetic requirements for four different heterogeneous electron-transfer reactions. 1) The

excited state chromophore dye complex must inject electrons into the photoanode at a rate that is faster than the competing reaction with the oxidized mediator. The electron injection process is complex but occurs on the femtosecond to picosecond time scale[18,19] while the reaction of the excited state dye with the oxidized form of the mediator occurs on the slower time scale of 10-100 ps.[20] 2) The oxidized dye must be reduced by the mediator faster than it recombines with the photo-injected electron. In the case of I^-/I_3^-, the reduction by the mediator occurs on the tens of picoseconds time scale while the back reaction of the photo-injected electron with the mediator occurs on the microsecond to millisecond time scale.[20] 3) The oxidized form of the mediator must react slowly with the electrons in both the TiO_2 and the fluorine-doped tin oxide contacts. 4) The reduction of the oxidized mediator at the cathode must also be fast (*vide infra).*

Despite the fact that there is no a priori way to determine whether a new mediator will meet all these requirements, there are important practical and fundamental reasons for investigating mediator systems other than I^-/I_3^-. The I^-/I_3^- couple is corrosive, volatile and compatible with only a few non platinum-group metals. It also has a significant absorbance in the visible region of the electromagnetic spectrum which lowers overall cell efficiency. Further, its redox potential is not well matched with the redox potential of the N3 dye. On a more fundamental level, the I^-/I_3^- couple is not modifiable so it provides no room for systematic study. An important reason for investigating new cobalt-based metal complex mediators is that they are chemically modifiable and allow for tuning redox properties to better match cell potential requirements and study the behavior of mediators while taking into account chemical modifications. The main types of modifications introduced are to vary the number and types of substituents on the bipyridine ligands.

Cobalt coordination complexes undergo slow self - exchange for the $Co^{2+/3+}$ oxidation states.[21] This is an important consideration in meeting kinetic requirement #3 described above. An outer –sphere redox couple undergoing rapid self-exchange would not be an effective DSSC mediator.[16,22] Since the Co II/III couple is slow, heterogeneous electron transfer should also be slow, as predicted by Marcus theory, and allow for cobalt complexes to meet the kinetic requirement for a mediator.[23-25]

Attempts to use cobalt complexes as replacements for the I^-/I_3^- mediator were largely unsuccessful until 2001 when Gratzel et al. reported using a novel Co II/III system.[14] The cells were designed using the standard operating characteristics described previously for "Gratzel" type cells excepting that the I^-/I_3^- mediator had been replaced with a mixture of the Co^{2+} and Co^{3+} forms of cobalt associated with bipyridine-like ligands in order to function as complex mediators. Efficiencies of 2.2% at 1 sun irradiation were reported which is 20% the efficiency of the standard I^-/I_3^- cells.[14] At approximately the same time Sapp et al. reported using polypyridine type ligands that demonstrated efficiencies about 80% of the standard I^-/I_3^- cells when certain types of substituents were appended to the polypyridine type ligands.[13] While Gratzel's ligand was a unique, highly unsymmetrical tridentate molecule not readily modified, the ligands developed by Sapp, et al. offered the possibility of tuning the redox potential of the ligands by modifying the ligand's steric and electronic properties. The cell efficiencies reported using these new cobalt complexes were shown to be dependent on how and in what positions the ligands are substituted.

Thus, in principle, it should be possible to improve the open circuit voltage of a cell mediated with a cobalt polypyridyl complex by introducing electron withdrawing substituents on the bipyridine ligands. Such substituents shift the potential of the $Co^{2+/3+}$ couple to more positive

values. Since, as stated above, the cell voltage is determined by the difference in the mediator redox potential and the Fermi energy of the electrons in the photoanode, a more positive $Co^{2+/3+}$ potential should improve cell efficiency. However, many of the other factors which go into determining the cell efficiency (e.g. the kinetics of the various electron transfer processes discussed earlier) can be affected by changes in the substituents on the bipyridine as well. In other words, ligand modifications made to move the complex to more positive potentials, for example, substituting bulky electron withdrawing groups tert-butylcarboxy ester and di-N,N-butylcarboxyamide at the 4- and 4'- positions for the electron donating *tert*-butyl, change other things.[13] For instance, both groups give the expected shift to more positive $Co^{2+/3+}$ potentials resulting in greater open circuit cell voltages, but the cyclic voltammograms of these complexes indicate that the electrode-dependent heterogeneous electron transfer rates are dramatically different relative to the tert-butylbipyridine complex.[13] Similar differences in other heterogeneous electron transfer processes associated with DSSCs also occur. As a consequence, cells mediated with cobalt complexes of 4,4'-di-*tert*-butylcarboxy ester 2,2'-bipyridine have significantly higher open circuit voltages and significantly lower short circuit currents than identical cells mediated by the 4,4'-di-*tert*-butylbipryidine complex resulting in a lower over-all efficiency.

In an effort to better understand which factors play the more important role it would be desirable to change the electron donating/withdrawing nature of a substituent without changing its structure (i.e., size and shape). While this is not strictly possible, it is in principle possible to change the electronic effect of a substituent without drastically changing its size. For example, CH_3 – and CF_3 – are roughly the same size but dramatically different in their electronic effects. The $Co^{2+/3+}$ potential of the 4,4'-substituted-2,2' bipyridines of these two ligands differs by ca.

600mV.[26] Unfortunately neither of these substituents is large enough to allow for appropriate rates of the various relevant heterogeneous electron transfers in DSSCs to function as reasonable mediators (*vide supra*). As a consequence, we undertook the attempted synthesis of halogenated analogs of 4,4'-bipyridines with large alkyl substituents. Fluorine and chlorine are obvious choices; however, for a variety of reasons outlined below, ligands with halogen substitutions on the α-carbon either were not successfully prepared or were too unstable to be isolated. As a fall back, the α-hydroxyl functional group was successfully introduced. While hydroxyl substitution does constitute a structurally larger perturbation than a halide substitution, it is not nearly as bulky as an ester or amine and has the advantage of being an easier synthetic substitution route than halide introduction (especially fluorine).

In the following chapter, various efforts are described to alter the redox potential of the cobalt complex mediator by substituting a halogen for hydrogen at the α-carbon. Bases of differing pKa, including amides, alkyl lithium bases, and amines, were employed in an attempt to remove the proton from the α-carbon. Also, a fluorinating agent intended to transfer F^+ to carbanions was also used in conjunction with the bases. Synthetic attempts designed to introduce a chlorine or bromine atom with chloro- and bromosuccinimides but resulting in a vinyl type elimination product will be described. Anhydrous hydrofluoric acid was used in an attempt to add fluorine at the α-carbon of this elimination product. Finally, the approach used to introduce a hydroxyl group at the α-carbon position is described.

ENDNOTES

(1) Nazeeruddin, M. K.; Pechy, P.; Renouard, T.; Zakeeruddin, S. M.; Humphry-Baker, R.; Comte, P.; Liska, P.; Cevey, L.; Costa, E.; Shklover, V.; Spiccia, L.; Deacon, G. B.; Bignozzi, C. A.; Gratzel, M. *Journal of the American Chemical Society* 2001, *123*, 1613-1624.

(2) Avrutin, V.; Izyumskaya, N.; Morkoc, H. *Superlattices Microstruct.* 2011, *49*, 337-364.

(3) Harder, N.-P.; Wurfel, P. *Semicond. Sci. Technol.* 2003, *18*, S151-S157.

(4) Tayebjee, M. J. Y.; Hirst, L. C.; Ekins-Daukes, N. J.; Schmidt, T. W. *J. Appl. Phys.* 2010, *108*, 124506/124501-124506/124507.

(5) Hillhouse, H. W.; Beard, M. C. *Curr. Opin. Colloid Interface Sci.* 2009, *14*, 245-259.

(6) Huang, S. Y.; Schlichthoerl, G.; Nozik, A. J.; Graetzel, M.; Frank, A. J. *J. Phys. Chem. B* 1997, *101*, 2576-2582.

(7) Nazeeruddin, M. K.; Kay, A.; Rodicio, I.; Humphry-Baker, R.; Mueller, E.; Liska, P.; Vlachopoulos, N.; Graetzel, M. *J. Am. Chem. Soc.* 1993, *115*, 6382-6390.

(8) Hagfeldt, A.; Graetzel, M. *Acc. Chem. Res.* 2000, *33*, 269-277.

(9) Bach, U.; Lupo, D.; Comte, P.; Moser, J. E.; Weissortel, F.; Salbeck, J.; Spreitzer, H.; Gratzel, M. *Nature (London)* 1998, *395*, 583-585.

(10) Savenije, T. J.; Warman, J. M.; Goossens, A. *Chem. Phys. Lett.* 1998, *287*, 148-153.

(11) Murakoshi, K.; Kogure, R.; Wada, Y.; Yanagida, S. *Chem. Lett.* 1997, 471-472.

(12) Murakoshi, K.; Kogure, R.; Wada, Y.; Yanagida, S. *Sol. Energy Mater. Sol. Cells* 1998, *55*, 113-125.

(13) Sapp, S. A.; Elliott, C. M.; Contado, C.; Caramori, S.; Bignozzi, C. A. *J. Am. Chem. Soc.* 2002, *124*, 11215-11222.

(14) Nusbaumer, H.; Moser, J.-E.; Zakeeruddin, S. M.; Nazeeruddin, M. K.; Graetzel, M. *J. Phys. Chem. B* 2001, *105*, 10461-10464.

(15) Oskam, G.; Bergeron, B. V.; Meyer, G. J.; Searson, P. C. *J. Phys. Chem. B* 2001, *105*, 6867-6873.

(16) Gregg, B. A.; Pichot, F.; Ferrere, S.; Fields, C. L. *J. Phys. Chem. B* 2001, *105*, 1422-1429.

(17) Hamann, T. W.; Jensen, R. A.; Martinson, A. B. F.; Van, R., Hal; Hupp, J. T. *Energy Environ. Sci.* 2008, *1*, 66-78.

(18) Lian, T.; Asbury, J. B.; Ghosh, H.; Weng, Y.-X.; Hang, K.; American Chemical Society, 1999, pp PHYS-361.

(19) Lian, T.; Ghosh, H.; Asbury, J. B.; American Chemical Society, 1998, pp PHYS-424.

(20) Kalyanasundaram, K.; Graetzel, M. *Micelles, Microemulsions, Monolayers*; Dekker: New York, NY, 1998.

(21) Sutin, N. *Prog. Inorg. Chem.* 1983, *30*, 441-498.

(22) Gregg, B. A. In *Semiconductor Photochemistry and Photophysics*; Ramamurthy, V., Schanze, K. S., Ed.; Marcel Dekker, Inc., 2003, pp 51-58.

(23) Hamann, T. W.; Farha, O. K.; Hupp, J. T. *J. Phys. Chem. C* 2008, *112*, 19756-19764.

(24) Klahr, B. M.; Hamann, T. W. *J. Phys. Chem. C* 2009, *113*, 14040-14045.

(25) Ondersma, J. W.; Hamann, T. W. *J. Phys. Chem. C* 2010, *114*, 638-645.

(26) Moss, C., Personal Communication.

CHAPTER 3.

A SUBSTITUTED BIPYRIDINE LIGAND FOR A COBALT (II/III) COMPLEX AS AN EFFICIENT ELECTRON-TRANSFER MEDIATOR IN DYE SENSITIZED SOLAR CELLS

Introduction

As stated above, the goal of this study was to tune the reduction/oxidation (redox) potential of the electron transfer mediator in a DSSC with minimal changes in the structure of the mediator, within the context of a ligand having a large enough substituent in the 4, 4' – position to function similarly to *tert*-butyl. For this purpose, 4-(3-pentyl)-bipyridine, shown in figure 1 was chosen. The 3-pentyl substituent is slightly larger than a tert-butyl group while having a hydrogen atom on the α-carbon that can, in principle, be replaced by an electron withdrawing group.

A fluorine atom is similar in size to a hydrogen atom (van der Waals radii are 120 and 147 pm, respectively, for hydrogen and fluorine) so substituting a fluorine atom for hydrogen would have minimal effects on the overall ligand size and steric considerations. Fluorine is an extremely strong electron-withdrawing group which will pull electron density from the ligand bipyridine rings toward fluorine. This more electron deficient ring will, in turn, draw electron density from the cobalt metal center to which it is coordinated making the metal more difficult to oxidize. Therefore the E^o of the cobalt II/III couple will become more positive relative to the complex with the corresponding ligand having a hydrogen substituent. If an electron donating group like CR_3 were appended to the bipyridine ring ligand a potential shift in the opposite direction would be realized. The open circuit cell voltage (Voc) of a DSSC is approximately the

potential difference between the conduction band of the photoanode and the potential of the Co II/III couple. When the potential of the Co II/III couple becomes more positive the Voc increases since the potential of the conduction band is negative relative to the Co II/III couple.

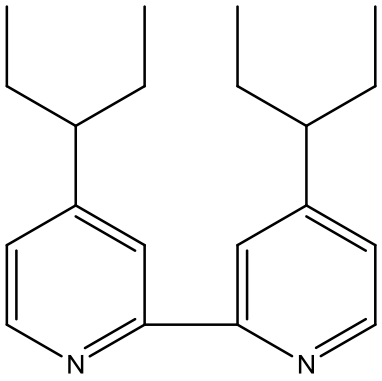

Figure 3-1. The structure of 4, 4'-(dipentan-3-yl)-2,2'-bipyridine, the ligand used for the metal complex employed as a sacrificial electron mediator in dye-sensitized solar cells.

4, 4'-(dipentan-3-yl)-2,2'-bipyridine is prepared by coupling two 4-(3-pentyl)-pyridines together[1]. Since the chemistry at the benzylic carbon should be approximately the same for the pyridine and bipyridine, the more readily available 4-(3-pentyl)- pyridine was used as a surrogate for the bipyridine in the following reactions in an attempt to find an appropriate synthetic route to substitution at the benzylic carbon. In general, a base was chosen to remove hydrogen from the benzylic position of 4-(3-pentyl)-pyridine. Deuterated water was later added to quench the reaction which should result in deuteration that would be evident by ^{1}H NMR.

Figure 2 is the ^{1}H NMR spectra for 4-(3-pentyl)-pyridine as obtained from AGC Chemical, Inc. at a reported purity of 95+%. There are clearly evident some impurity peaks in the spectrum but the sample is predominantly the desired pyridine. There are two pairs of differing aromatic hydrogens which are located between 7.0 ppm and 9.0 ppm. The single

hydrogen attached to the α-carbon is seen at 2.4 ppm. The remaining alkyl hydrogens are downfield of the α-carbon hydrogen and are located in the region of the spectrum between 0.5 ppm and 2.0 ppm.

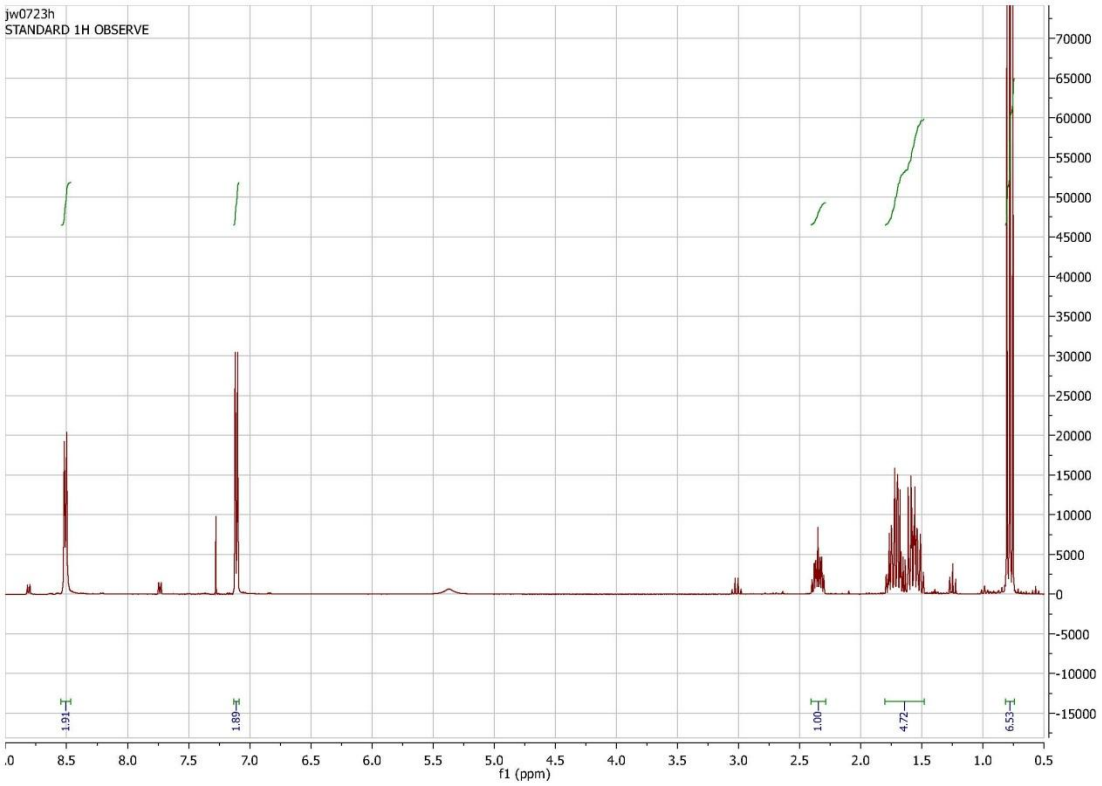

Figure 3-2. ^{1}H NMR spectrum for 4-(3-pentyl)-pyridine.

The following section describes the experimental conditions used in the attempts to obtain the substitution product where the α-carbon hydrogen is replaced. The section headings indicate the type of base used. The Results and Discussion section pertaining to the synthetic approaches follows.

Experimental Section

Materials. Acetonitrile (Fisher Optima Grade) was dried over molecular sieves prior to use as solvent for electrochemical experiments. All other solvents (Fisher ACS Grade) were used as received. 4-(3-pentyl)-pyridine (TCI 95+%) was also used as obtained. 4,4'-Dimethyl-2,2'-bipyridine (DMB) was purchased from Reilley Industries, Indianapolis and recrystalized from ethyl acetate. Tetrahydrofuran (THF) was dried and freshly distilled prior to each use by refluxing under nitrogen over sodium/benzophenone. All other chemicals were purchased from Aldrich and used as received.

Sodium amide. 110 mg of sodium amide (0.95 eq.) were dissolved in 6 mL of dry THF. The solution was saturated with sodium amide with the undissolved fraction appearing as a white solid in the bottom of the flask. The reaction vessel was kept under positive nitrogen pressure at -78 ºC (dry ice/acetone). Addition of 0.5 mL of 4-(3-pentyl)-pyridine (1.0. eq.) resulted in the solution turning a light peach color. After two hours reaction time with stirring, 0.25 mL of deuterium oxide (D_2O – 1eq.) was added to quench the reaction. Excess D_2O formed solid ice in the reaction vessel. The solvent and excess D_2O were removed by rotary evaporation. The ^1H NMR spectra was obtained with a Bruker 300MHz using deuterated chloroform solvent. The resulting spectrum is shown in figure 3.

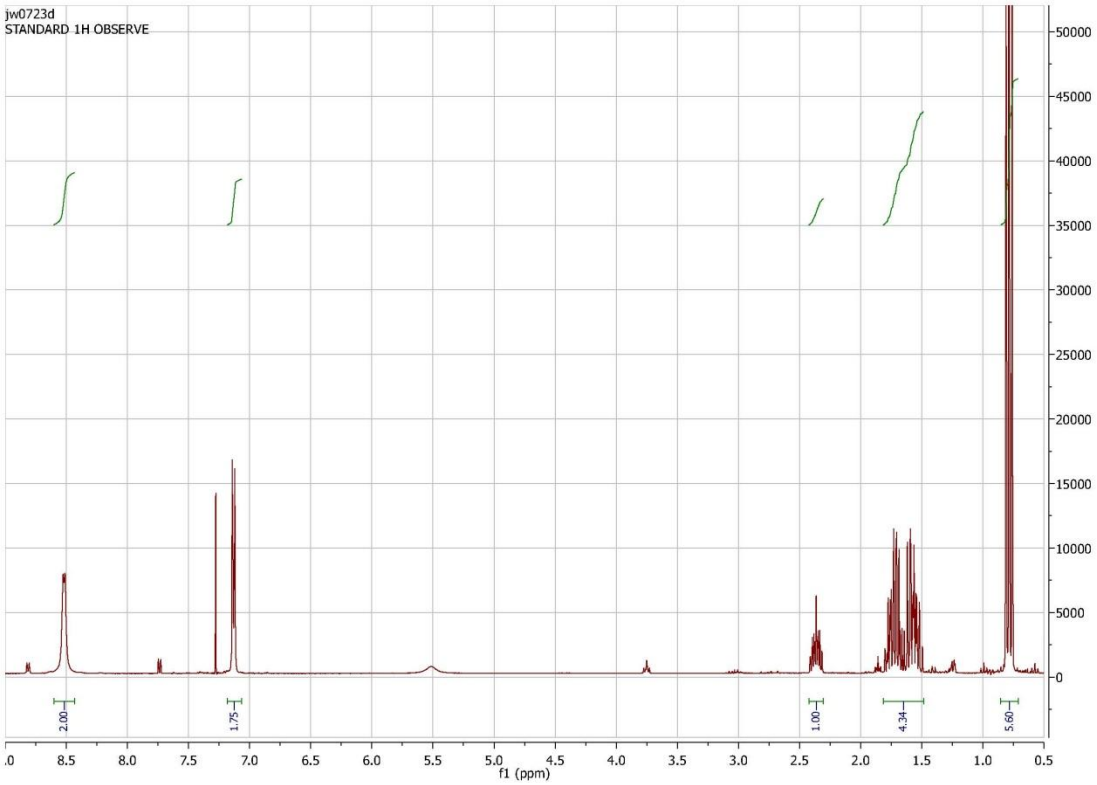

Figure 3-3. ^{1}H NMR spectrum for 4-(3-pentyl)-pyridine after attempted deprotonation at the benzylic position with sodium amide at -78 ºC followed by quenching with D_2O.

The same reaction was repeated at room temperature by adding 70 mg of sodium amide (0.95 eq.) to 6.0 mL of dry, freshly distilled THF. 0.3 mL of 4-(3-pentyl)-pyridine (1.0 eq.) were added leaving the solution a pale yellow. Most of the sodium amide remained undissolved. After 3 hours, the solution appeared orange with nearly all sodium amide dissolved but a very small amount of solid remained. Quenching with 0.25 mL of yielded an orange solution which showed no evidence of undissolved solids. After rotary evaporation of solvent, the reaction product was redissolved in deuterated chloroform solvent and examined by ^{1}H NMR. The spectrum obtained is figure 4 below.

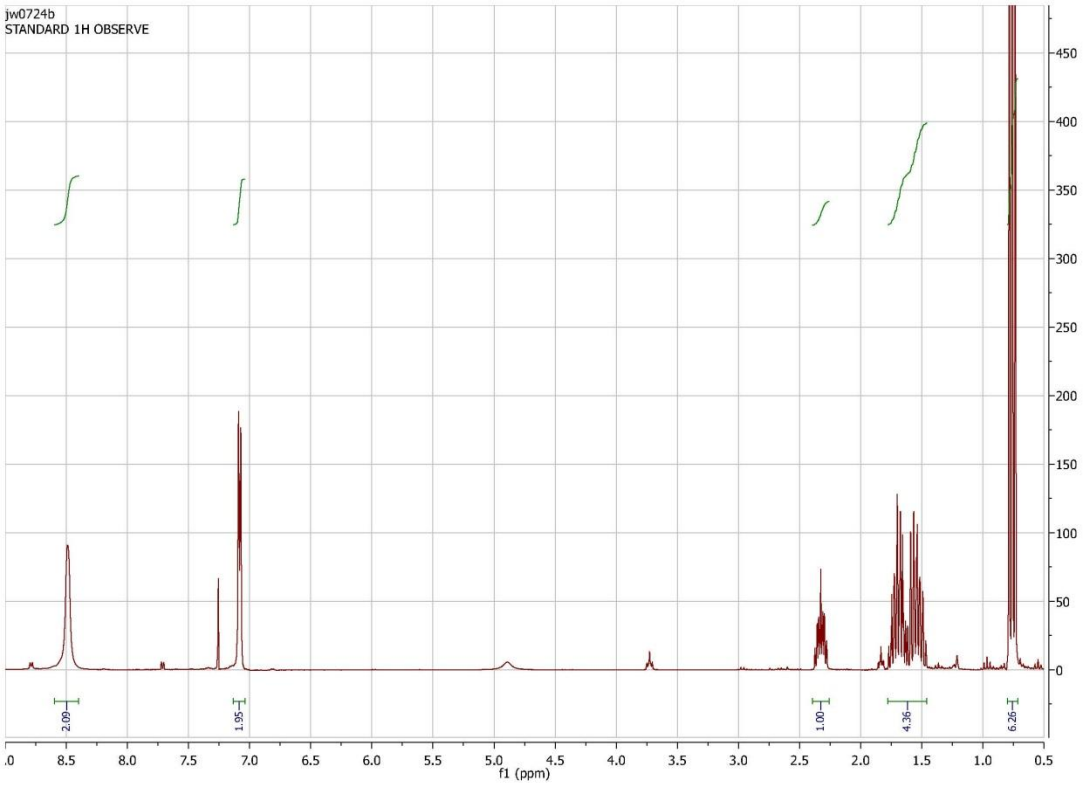

Figure 3-4. The ^{1}H NMR spectrum for 3-isopentyl pyridine after attempted deprotonation at the benzyl position with sodium amide at 25 ºC followed by quenching with D_2O.

Methyllithium. 0.3 mL of 4-(3-pentyl)-pyridine (1.0 eq.) were added to dry THF in a reaction vessel purged of oxygen with streaming nitrogen and kept under positive nitrogen pressure. The reaction vessel was kept at -94° C with a hexane / liquid nitrogen slurry. 1.1 mL (0.95 eq.) of methyllithium were added, turning the solution yellow over the course of 30 minutes. Gas evolution was witnessed as the reaction was quenched with D_2O. As the solution was warmed to room temperature the solution remained a very pale yellow color as a white precipitate coated the bottom of the flask. The solid is most likely LiDO and did not appear to contain pyridine by NMR. After rotary evaporation of solvent, the yellow oil from the reaction was examined using ^{1}H and ^{2}H NMR. The ^{1}H NMR spectrum is shown in figure 5 below.

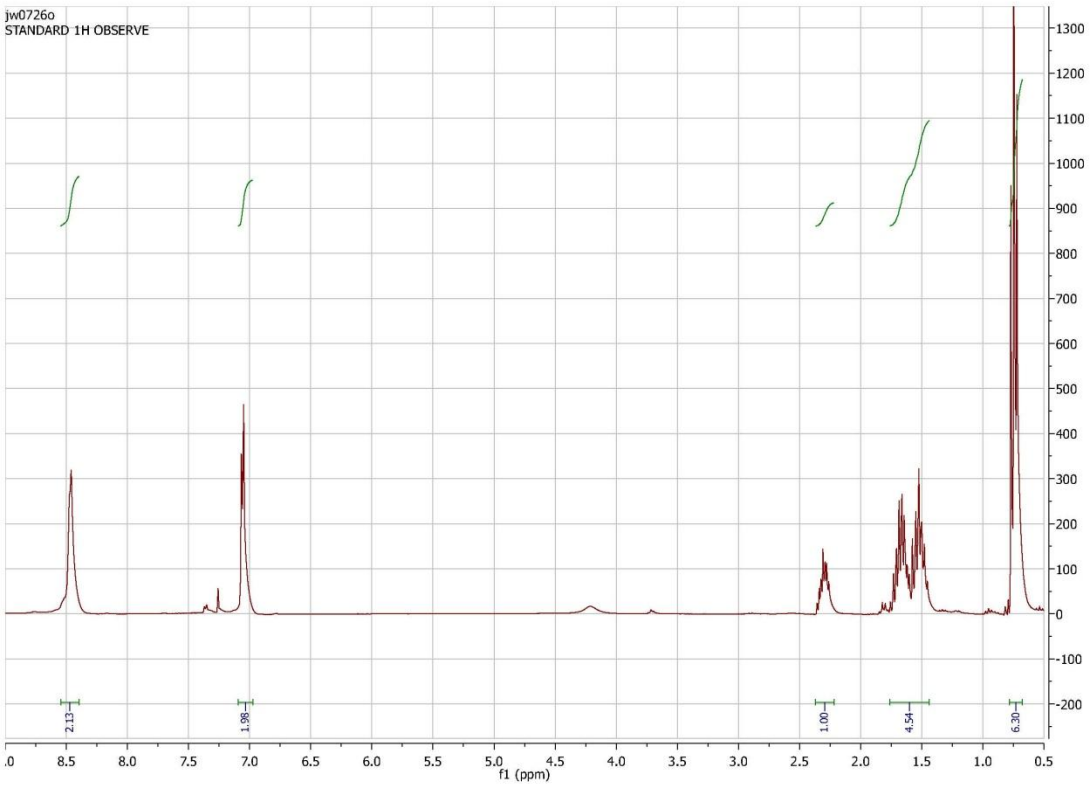

Figure 3-5. The ^{1}H NMR spectrum for 3-isopentyl pyridine after attempted deprotonation at the benzyl position with methyllithium at -78 ºC followed by quenching with D_2O.

n-Butyllithium. 0.3 mL of 4-(3-pentyl)-pyridine (1.0 eq.) were added to dry THF in a reaction vessel purged of oxygen with streaming nitrogen and kept under positive nitrogen pressure. The reaction vessel was kept at -94° C as with the methyllithium reaction. 3.7 mL (0.95 eq.) of n-butyllithium were added which turned the resulting reaction mixture orange. The deuterated water added to quench the reaction froze upon addition. As the ice melted the reaction mixture became yellow and eventually appeared colorless after the entire volume of ice melted. As the D_2O melted a white precipitate formed. The white precipitate was dried under vacuum overnight and then examined with ^{1}H NMR and ^{2}H NMR (Figures 6&7).

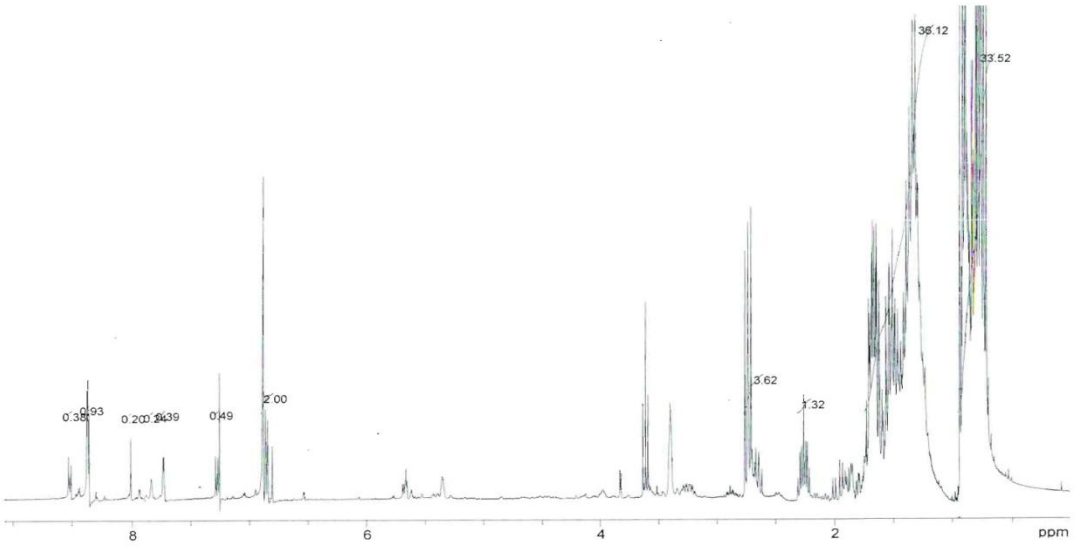

Figure 3-6. The ^{1}H NMR spectrum for 3-isopentyl pyridine after attempted deprotonation at the benzylic position with n-butyllithium at -78 ºC followed by quenching with D_2O.

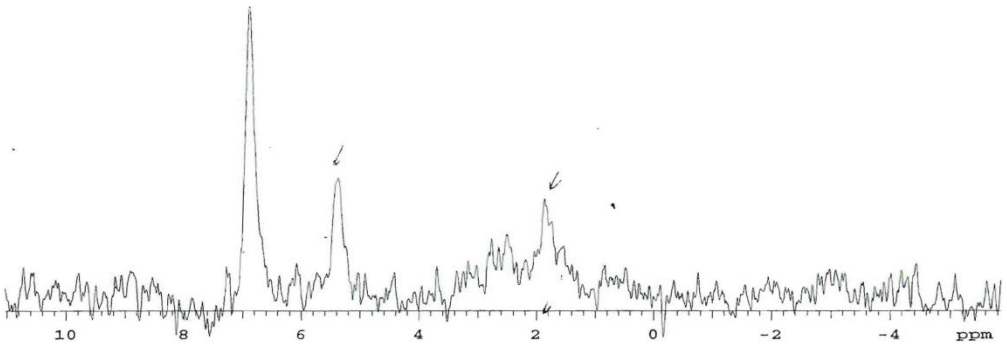

Figure 3-7. The ^{2}H NMR spectrum for 3-isopentyl pyridine after attempted deprotonation at the benzyl position with n-butyllithium at -78 ºC followed by quenching with D_2O.

Lithium propylamide. 0.152 mL of propylamine (0.95 eq. - Aldrich, 98%) was added to dry THF. The reaction vessel was purged of oxygen with streaming nitrogen, kept under positive nitrogen pressure, and cooled to -78° C with a bath of dry ice in acetone. 0.74 mL (0.95 eq.) of n-butyllithium was added in order to lithiate the propylamine. After one hour of stirring the lithium propylamide solution remained colorless. 0.3 mL of 4-(3-pentyl)-pyridine (1.0 eq.) was added producing a pale yellow color which became brighter over the course of 90 minutes. The reaction was quenched with D_2O. The solution became colorless as the deuterated ice melted. After removing solvent by rotary evaporation and drying in a vacuum oven overnight, the reaction product was analyzed by GC/MS.

Vinyl Grignard. 0.3 mL of 4-(3-pentyl)-pyridine (1.0 eq.) were added to dry THF in a reaction vessel purged of oxygen with streaming nitrogen and kept under positive nitrogen pressure. The reaction vessel was kept at -78° C by using a dry ice in acetone bath. 1.8 mL of vinyl Grignard reagent (0.97 eq.) were added and after 90 minutes an aliquot of the reaction mixture was added to D_2O under nitrogen. The reaction vessel was allowed to warm to 0° C in an ice water bath. After 60 minutes another aliquot was quenched with D_2O under nitrogen. Finally the reaction was allowed to proceed at room temperature for another 12 hours before quenching with D_2O (1.1 eq.). After removing solvent by rotary evaporation a milky, slimy precipitate remained. Dichloromethane was used to extract the product from this precipitate which left behind a small amount of solid. The liquid organic phase was allowed to concentrate by evaporation at room temperature before being analyzed by GC/MS.

n-Fluorobenzenesulfonimide(NFSI). 0.3 mL of 4-(3-pentyl)-pyridine (1.0 eq.) were added to dry THF in a reaction vessel purged of oxygen with streaming nitrogen and kept under positive nitrogen pressure. The reaction vessel was kept at -78° C by using a dry ice in acetone bath. 1.1 mL (0.95 eq.) of methyllithium were added, turning the solution yellow over the course of 30 minutes. After one hour, 0.583 g of NFSI (1.0 eq.), dissolved in THF, was added via canula to the reaction mixture. The solution was stirred for 15 minutes before removing the vessel from the cold bath for 10 minutes. The vessel was still cold as evidenced by frost forming on the sides. D_2O was added prior to the solvent being removed by rotary evaporation. The reaction product was red to brown in color and appeared to be a suspension in an orange liquid which was dried under vacuum overnight.

n-Chlorosuccinimide 0.3 mL of 4-(3-pentyl)-pyridine (1.0 eq.) and 237 mg of n-chlorosuccinimide(NCS) (0.97 eq.) were combined in a 100 mL round bottom flask with 50 mL of carbon tetrachloride solvent. The reaction mixture was stirred for 18 hours while being exposed to the ultraviolet (UV) light output from a UV lamp. No reaction was evidenced by NMR so the reaction conditions were modified slightly. An overhead projector lamp was used as a light source and 0.05 equivalent benzoyl peroxide (BPO) was added to the solution. BPO is a radical initiator which produces radicals under mild conditions. The 0.05 equivalent of BPO would produce 0.10 equivalent of initiator as each BPO decomposes to two radicals. The reaction was allowed to proceed for 12 hours but again no evidence of product was seen in the NMR spectrum. In order to determine if it was possible to chlorinate an alkyl group appended to the pyridine ring under the described conditions, 1eq of 4,4'-dimethyl-2,2'-dipyridyl, 2 equivalents of NCS, and 0.05 equivalent of BPO were combined in carbon tetrachloride and allowed to reflux for twelve hours. Reaction products were analyzed with TLC using a mobile phase of 5% acetone in methylene chloride. Finally, 1eq of 4-(3-pentyl)-pyridine, 1 equivalent of NCS, and 0.05 equivalents of BPO were combined in carbon tetrachloride and allowed to reflux for times varying from six to twelve hours. Reaction products were analyzed with TLC, using the same acetone : methylene chloride ratio as before, and by GC/MS.

n-Bromosuccinimide. 0.2 mL of 4-(3-pentyl)-pyridine (1.0 eq.) and 220 mg of n-bromosuccinimide(NBS) (1.0 eq.) were combined in a 100 mL round bottom flask with 50 mL of carbon tetrachloride solvent. The solution was gently stirred for 12 hours while being exposed to the light output of a standard overhead projector lamp. As the reaction proceeded, yellow succinimide solids were observed floating on the surface of the carbon tetrachloride. The solids

were separated from the mother liquor using vacuum filtration and a medium porosity frit. Neat carbon tetrachloride was used to rinse the solids. Methylene chloride was used to extract the product from the mother liquor.

Attempted fluorination of (E)-4-(pent-2-en-3-yl)pyridine. The reaction vessel used was a stainless steel cylinder closed at one end and threaded at the other end to connect to a vacuum line. The threaded end also has a seal in order to get a tight fit and not allow air to leak into or out of the cell. Below the threaded fitting is a valve used to contain the contents in the vessel when it is not connected to a vacuum line. 23 mg of (E)-4-(pent-2-en-3-yl)pyridine were added to the reaction vessel along with 3 mL of dry THF and a stir bar. The THF solution was frozen and evacuated of air on a vacuum line. The solution was allowed to thaw and degas. This process was repeated two more times to obtain a solution free of dissolved gases. The vessel was connected to a Schlenk line and frozen in a dry ice in acetone bath. Anhydrous hydrofluoric acid (HF) was introduced in to the line and allowed to condense in the reaction vessel. As the HF condensed the reaction mixture turns blackish purple. It was difficult to be certain but there did not appear to be a precipitate. The reaction vessel was sealed, removed from the Schlenk line and stirred for 18 hours at room temperature. After reconnecting the vessel to the vacuum line the HF and solvent were allowed to enter the vacuum line and condense into a second vessel which was cooled with a dry ice/acetone bath. After 5 hours about 1.5 mL of HF and solvent were collected while approximately 2 mL of solvent remained in the reaction vessel. The vessel was disconnected from the line and the contents delivered to a flask where it was neutralized using an aqueous sodium carbonate solution until neutral by pH paper. More sodium carbonate solution was used to raise the pH to 8 at which time a dark green to black precipitate was observed

separating from the green liquid. The liquid volume was now approximately 22 mL. The solids were separated from the liquid by vacuum filtration over a fine frit and vacuum dried for 12 hours. The dried solids were dissolved in dichloromethane solvent and were found to be mostly soluble. After filtering off the remaining solid, the solvent was removed by rotary evaporation to leave a green film with dark green to black solids. Deuterated chloroform was added in order to obtain the ^{1}H NMR spectrum shown in figure 8.

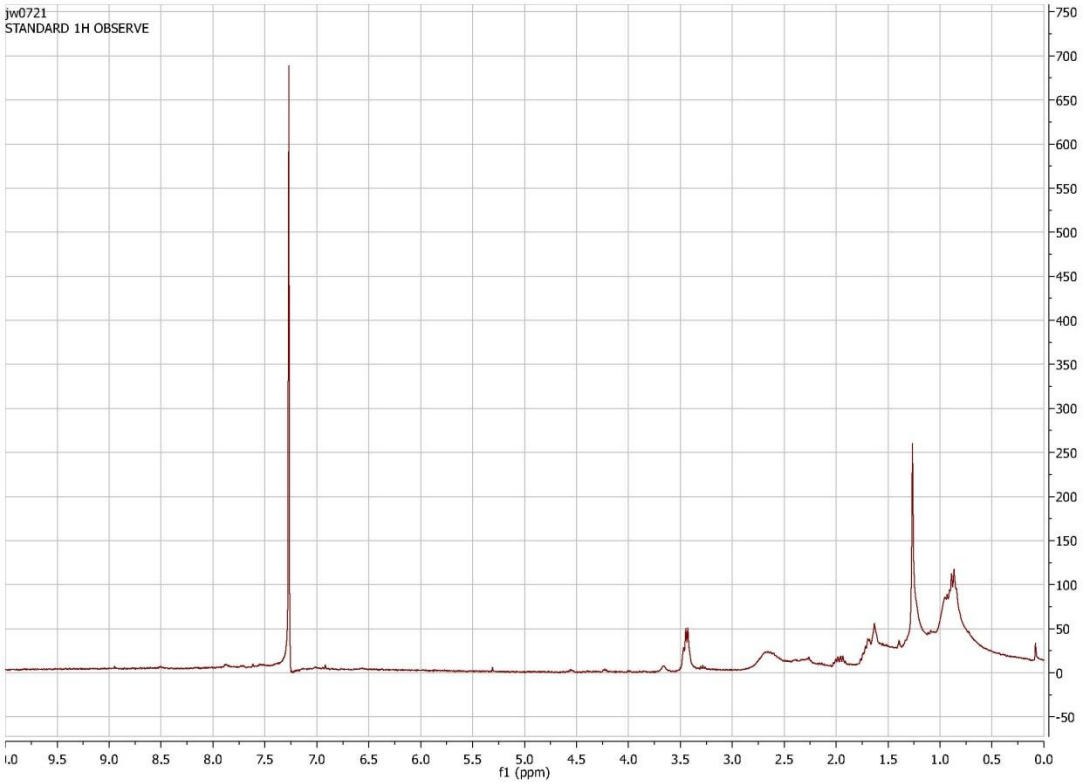

Figure 3-8. The ^{1}H NMR spectrum obtained from the attempt to fluorinate (E)-4-(pent-2-en-3-yl)pyridine with HF.

Synthesis of 3,3'-([2,2'-bipyridine]-4,4'-diyl)bis(propan-2-ol). To determine the feasibility of the 4, 4'-diisopropyl-2,2'-bipyridine oxidation, 4-isopropylpyridine was oxidized

with permanganate in a 1:1 methanol:water solvent mixture in order to introduce a hydroxyl group at the benzyl position. For 1:1 reaction stoichiometry, 3 equivalents of 4-isopropylpyridine were used with 2 equivalents of permanganate. The reaction was followed by monitoring the color of the reaction mixture. The permanganate reactant in the following half reaction has the familiar distinct purple color while the manganese (IV) oxide solid product is brown.

$$MnO_4^-(aq) + 4H^+ + 3\,e^- \leftrightarrow MnO_2(s) + 2\,H_2O$$

No evidence of the permanganate reduction, and thus oxidation of the pyridine, was observed at room temperature or by warming the reaction with warm tap water. Little (~30% by TLC) evidence of permanganate reduction was observed after 2 days of stirring at ambient temperature. The reaction was noted to be ~90% complete after 1.5 hours of reflux. The hydroxyl product, 3,3'-([2,2'-bipyridine]-4,4'-diyl)bis(propan-2-ol) (figure 9), was produced from 0.6 g of 4, 4'-diisopropyl-2,2'-bipyridine (3 eqs.) and 0.6 g of potassium permanganate (4.5 eq. of permanganate) in a 1:1 mixture of tert-butanol in water as a reaction solvent. Tert-butanol was substituted for methanol in order to prevent the oxidation of the alcohol. The ^{1}H NMR spectrum shown in figure 10 is of the hydroxyl product, 3,3'-([2,2'-bipyridine]-4,4'-diyl)bis(propan-2-ol). The benzylic proton, absent here, would be found at approximately 3 ppm

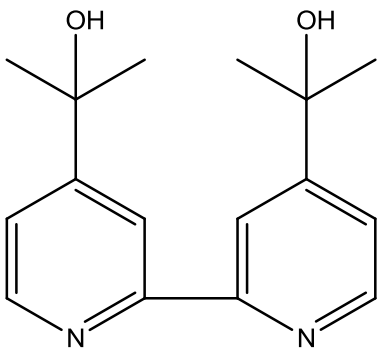

Figure 3-9. The ligand 3,3'-([2,2'-bipyridine]-4,4'-diyl)bis(propan-2-ol) in the cobalt metal complex used as an electron transfer mediator.

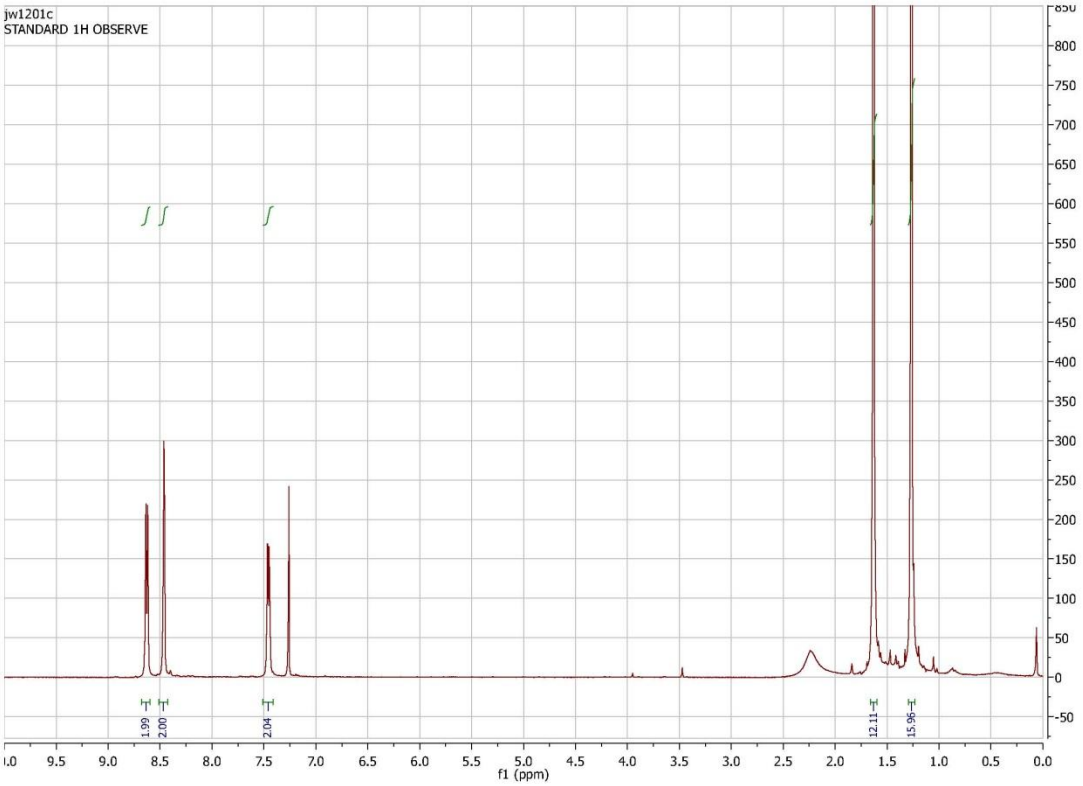

Figure 3-10. The ^{1}H NMR spectrum of 3,3'-([2,2'-bipyridine]-4,4'-diyl)bis(propan-2-ol).

Electrochemical setup. Cyclic voltammetry was performed using a glassy carbon ($7.1x10^{-2}$ cm^2) working electrode (BAS) and a platinum wire counter electrode employing an EG&G PAR Model 173 Potentiastat/Galvonstat controlled by a Model 175 Universal Programmer. All measurements were taken using a 0.1 M tetrabutylammoniumhexafluorophosphate ($TBAPF_6$) supporting electrolyte in acetonitrile (Optima Grade) which had been dried over molecular sieves. The potential was scanned from -0.2 V to 0.5 V at a sweep rate of 100 mV/s. The sensitivity of the potentiostat was set to 10 μA/V.

Dye Solutions. Saturated solutions of N3 dye [2] were prepared by adding ca. 5 mg of dye to 25 mL of dry ethanol. 200 mg of chenodeoxycholic acid were added in order to increase the solubility of the N3 dye. The saturated solution was sonicated 10-15 minutes and then filtered to remove any undissolved dye.

Electrode Preparation. TiO_2 colloidal solutions were prepared according to the method described by Zaban et al[3]. Films of the colloid were coated onto SnO_2:F coated glass electrodes (Pilkington TEC 15) by the "one scotch" method detailed by Zaban et al[3]. The films were allowed to air dry and then sintered in air at 450 ºC for one hour. The still hot electrodes (ca. 150 ºC) were immersed in the dye solution and allowed to soak in the absence of light for 12-18 hours. Prior to use, the photoanodes and gold cathode were rinsed with dry ethanol from a freshly opened bottle and then dried under flowing nitrogen.

Mediator Preparation. The cobalt mediator complex was prepared to have a concentration of 0.15 M by dissolving 19.9 mg of the hydroxyl isopropyl bipyridine (3 eq) and 13.5 mg of cobalt

(II) perchlorate hexahydrate (1 eq) in *gamma*-butyrolactone in order to make 250 μL of solution. This solution also contained 7.4 μL of t-butylpyridine (0.2 M) and 7.8 mg of lithiumtriflate (0.2 M). Nitrosoniumtetrafluoroborate at a concentration of 0.15 M *gamma*-butyrolactone was used as an oxidizing agent to insure that both forms of the Co II/III complex redox couple were present in the solution.

Results and Discussion

Initial attempts to remove a proton from the α-carbon of 4-(3-pentyl)-pyridine were made with sodium amide at a reaction temperature of -78 ºC. The ^{1}H NMR spectra shown in figure 3 reveals no deprotonation as the spectra obtained before and after the procedure appear to be very nearly identical. Specifically, the hydrogen attached to the α-carbon which appears at 2.4 ppm appears to be unaffected. Dueterated water was used to quench the reaction, which should have placed a deuterium on the alpha carbon. However, the integration of the area under the peak representing the alpha carbon proton still integrates to one. In response to this result, this reaction using sodium amide as the base was repeated with the temperature elevated to room temperature in order to promote the removal of the alpha carbon proton. Again there was no evidence of a deuterium replacing hydrogen in the NMR spectra shown in figure 4, as the number of protons attached at the alpha position was practically unchanged based on the results of the integration.

Methyllithium (pK_a ~50), a base with a comparable pK_a to sodium amide (pK_a ~ 38), was chosen in order to abstract the hydrogen at -94° C. Figure 5 indicates no deprotonation occurred at this temperature as again the peak at 2.4 ppm appears to be virtually unchanged. The reaction product was further examined by ^{2}H NMR and no peaks appreciably emerged from the baseline after 200 scans which would correspond to deuterium (Figure 7). Lithium propylamide was substituted for the methyllithium base at reaction temperatures of -78° C and 25 ºC and again no

evidence of deprotonation was observed by NMR or GC/MS. The stronger base n-butyllithium (pK_a ~ 40) removed protons from the pyridine with no selectivity. In fact it was hard to determine exactly where protons were removed as the spectrum shown in figure 6 was dramatically different than the starting material. The proton peaks seen in ^1H and ^2H NMR should appear at the same location on the ppm axis. Two peaks arise in the ^2H spectrum, shown in figure 7, which are located upfield of both the ring protons and the benzylic proton. The NMR results indicate a base that is more basic than methyllithium at -94° C and less basic than n-butyllithium at -94° C is required. This led me to try methyllithium at -78° C for a longer reaction time. The resulting ^1H NMR of the reaction product matched the spectrum of the 4-(3-pentyl)-pyridine starting material in that the presence of an α-carbon hydrogen was seen in equal amounts in both spectra. The ^2H NMR was problematic in that a sufficient lock level was difficult to obtain. However, after 192 scans no evidence of a deuterium signal was present and no peaks emerged from the baseline leading to the conclusion that the benzylic hydrogen was unaffected and not replaced by deuterium.

Vinyl Grignard reagent was used to try and remove the benzylic proton. Using similar reaction conditions as before (-78° C) as well as increasing the temperature to 0 ºC and ultimately to 25 ºC provided no evidence of benzylic substitution. Results of GC-MS show that at least 86% of the 4-(3-pentyl)-pyridine was un-reacted and no other reaction products were as much as ten percent abundant. The main reaction product, having an abundance of nine percent, was found to have a mass of 134 amu compared to the 4-(3-pentyl)-pyridine parent which has a mass of 149 amu.

If methyllithium was removing the benzylic hydrogen to any extent it should be possible to fluorinate the carbanion with N-fluorobenzenesulfonimide(NFSI) which has the chemical

formula $(C_6H_5SO_2)_2NF$. NFSI is a stable, crystalline material which readily transfers F^+ to enolates and carbanions[4]. In an attempt to accomplish this fluorine cation transfer to the benzyl position, the methyllithium deprotonation reaction was repeated at -78° C. After one hour of contact between the pyridine and methyllithium, a solution of NFSI dissolved in dry THF was added to the reaction mixture via canula to avoid contact with the atmosphere. This reaction product was compared with the starting material using thin layer chromatography (TLC). The mobile phase was 10 mL of a 1:1 mixture of dichloromethane and cyclohexane to which two drops of concentrated ammonium hydroxide were added. TLC plates were exposed to ammonia vapor for several minutes prior to being introduced to the mobile phase in a sealed resolution chamber. The retention factor (Rf) for NFSI was measured to be 0.1. The Rf for the un-reacted 4-(3-pentyl)-pyridine was 0.9. The reaction product was found to have a Rf of 0.5. This reaction product was examined by gas chromatography coupled to a mass spectrometer (GC-MS). After a two minute delay, the temperature of the chromatograph chamber was ramped from 80 ° C to 180 ° C over the course of ten minutes. One predominant peak (93%) was noted at a three minute retention time which was a fragment of the 4-(3-pentyl)-pyridine starting material. No other reaction product was as much as three percent abundant. This deprotonation with subsequent hydrogen replacement by fluorine reaction was repeated with the reaction mixture allowed to warm to 25 ºC while stirring for two hours in an oxygen free environment. GC/MS of the resulting product showed 79% of the starting material to be un-reacted. The next major fraction, which did not match the mass per charge ratio of the desired product was 12% abundant.

An attempt was made to chlorinate or brominate the pentyl pyridine with n-bromosuccinimide(NBS) or n-chlorosuccinimide(NCS). Multiple attempts were made at chlorination. After initial attempts were unsuccessful, the reaction was repeated using new

sources of NCS, increasing reaction times, and while introducing the radical initiator BPO both at the start of the reaction and over time. In each case, little to no evidence of chlorine substitution was seen in the NMR scans. As a test for proof of concept, 4,4'-dimethyl-2,2'-dipryridyl (DMB) was chlorinated using NCS and the radical initiator BPO. When refluxing for 24 hours while adding more BPO after 12 hours, the methyl hydrogens integrated to 3.6 (from 6.0) with two substitution products present as analyzed by TLC. All three fractions obtained from the reaction mixture, presumably two substitution products and unreacted DMB, were positive to an iron test. The iron test introduces a dilute aqueous ferrous perchlorate solution to bipyridine substituted ligands from the reaction mixture. Iron (II) bipyridyl complexes exhibit a distinct red color on silica gel coated glass TLC plates. The analogous reaction using NBS produced similar results. Despite the reaction products being successfully isolated to about 90 percent purity by extraction with methylene chloride, the GC/MS data indicated the halogen was eliminating at the vinyl position and yielding the alkene, 4,4'-di((E)-pent-2-en-3-yl)-2,2'-bipyridine (figure 11). To check the feasibility of fluorinating the bipyridine, an attempt to fluorinate (E)-4-(pent-2-en-3-yl)pyridine across the carbon-carbon double bond was made using anhydrous hydrofluoric acid. However, the resulting spectrum from a ^{19}F NMR probe indicated no sign of fluorine.

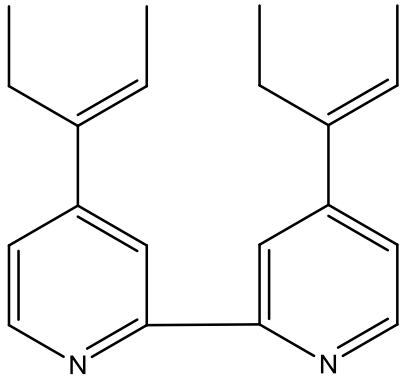

Figure 3-11. The elimination product 4,4’-di((E)-pent-2-en-3-yl)-2,2’-bipyridine obtained from the attempted halogenations at the benzylic position of 4, 4’-(dipentan-3-yl)-2,2’-bipyridine.

Ultimately, 4, 4’-diisopropyl-2,2’-bipyridine, which is structurally similar to 4, 4’-(dipentan-3-yl)-2,2’-bipyridine, was oxidized by replacing the benzylic hydrogen with the electron withdrawing hydroxyl group in order to determine if the hydroxyl group would have a similar effect on the DSSC voltage as a fluorine. 4-(isopropyl)-pyridine was oxidized with potassium permanganate in order to determine a reasonable set of reaction conditions for the oxidation of 4, 4’-diisopropyl-2,2’-bipyridine. The oxidation of the bipyridine to the hydroxyl product, 3,3’-([2,2’-bipyridine]-4,4’-diyl)bis(propan-2-ol), shown in figure 9, was accomplished by refluxing the bipyridine with potassium permanganate in a mixture of tert-butanol and water.

The cyclic voltammogram for the cobalt 4, 4’-diisopropyl-2,2’-bipyridine complex is shown in figure 12. The cathodic peak was found to reach a maximum at 260 mV while the anodic peak was located at 144 mV resulting in an $E_{1/2}$ for the Co II/III couple for this complex of 202 mV. The cobalt 3,3’-([2,2’-bipyridine]-4,4’-diyl)bis(propan-2-ol) complex had the cathodic peak at 282 mV and the anodic peak located at 162 mV for an $E_{1/2}$ of 222 mV for the Co II/III couple as seen in figure 12.

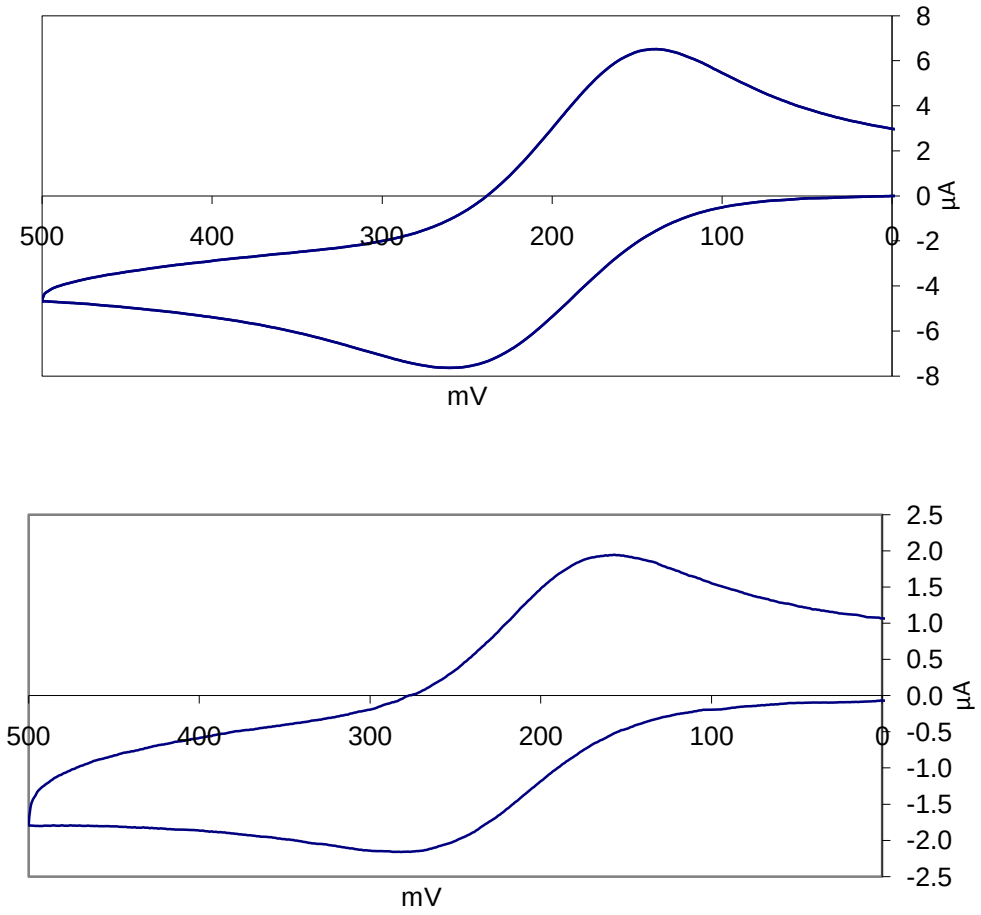

Figure 3-12. Cyclic voltammograms of the cobalt 4, 4'-diisopropyl-2,2'-bipyridine complex (above) and the cobalt 3,3'-([2,2'-bipyridine]-4,4'-diyl)bis(propan-2-ol) complex (below).

The current-voltage (iV) curves (figure 13) for standard mesoporous "one scotch" photoanodes dyed with N3 dye in conventional DSSC configurations[3] employing the cobalt 4, 4'-diisopropyl-2,2'-bipyridine complex (above) and the cobalt 3,3'-([2,2'-bipyridine]-4,4'-diyl)bis(propan-2-ol) complex (below) mediators as described in the experimental section above were measured at 100 mW cm^{-2} (~1 sun) illumination. The voltage was scanned to 0.6 V in both cases as previously measured cells did not display open circuit voltages (Voc) greater than 600 mV [1]. This potential window was not wide enough to reach the open circuit voltage. The Voc for

the hydroxyl ligand was approximated by the best linear fit line for the tailing portion of the more negative voltages. This approximation was necessary because there was not enough cobalt complex with the hydroxyl substituted ligand prepared to repeat the measurement at subsequent times. The DSSSC utilizing the cobalt complex containing hydroxyl substituted ligands realized an appreciably higher photovoltage of approximately 0.64 V relative to 0.52 V for the cobalt complex with diisopropyl bipyridine ligands. The fill factor of 58% for the hydroxyl ligand was also higher than the 52% fill factor for the cobalt diisopropyl bipyridine complex. Of concern is the lower current displayed by the cell employing the cobalt complex with the hydroxyl substituted ligands.

a)

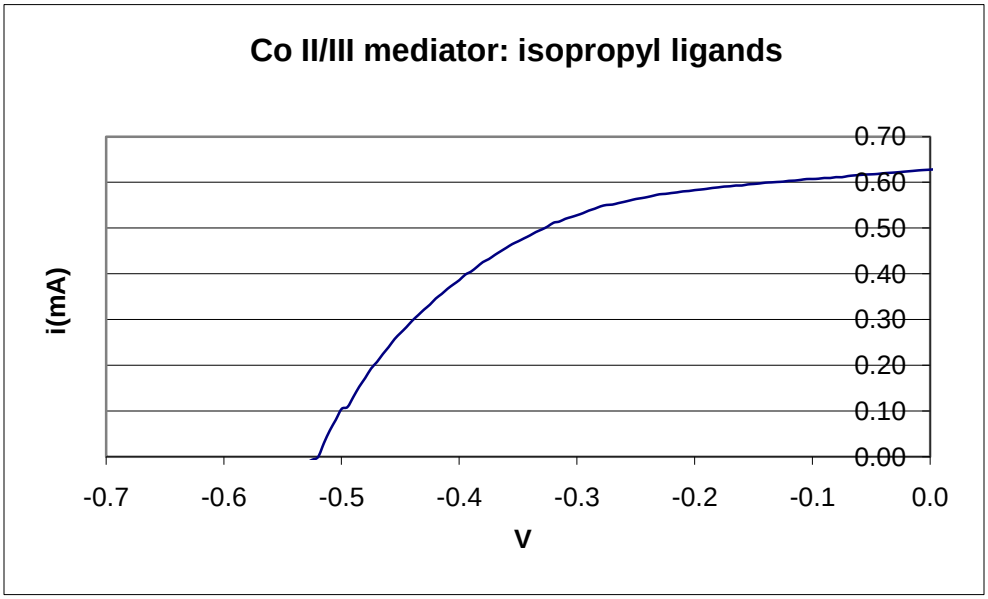

b)

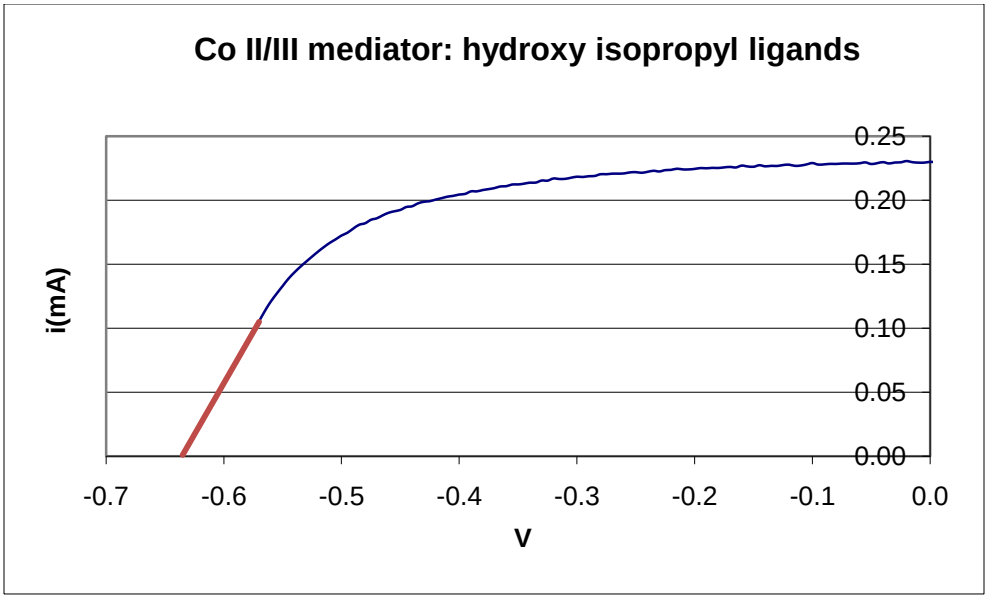

Figure 3-13. Potential vs. voltage curves for DSSCs utilizing cobalt complexes with a) diisopropyl ligands and b) hydroxyl substituted ligands.

Conclusion

The $E_{1/2}$ of the cobalt II/III couple shifted to a potential 22 mV more positive for the complex employing the hydroxyl substituted ligand. In spite of this relatively small change in potential, the hydroxyl substituted diisopropyl bipyridine ligand displayed a larger Voc and fill factor relative to the unsubstituted diisopropyl bipyridine ligand when used as a cobalt complex mediator in DSSCs employing standard conditions in all other respects.

ENDNOTES

(1) Sapp, S. Ph. D. Dissertation, Colorado State University, 2002.

(2) Nazeeruddin, M. K.; Kay, A.; Rodicio, I.; Humphry-Baker, R.; Mueller, E.; Liska, P.; Vlachopoulos, N.; Graetzel, M. *J. Am. Chem. Soc.* 1993, *115*, 6382-6390.

(3) Zaban, A.; Ferrere, S.; Sprague, J.; Gregg, B. A. *Journal of Physical Chemistry B* 1997, *101*, 55.

(4) *Aldrichimica Acta* 1995, *28*, f36.